Effects of Tide and Wave on the Transport of Water and Sediments off the Yellow River Mouth in Winter

Xinyue Cheng[1, 2, 3], Jianrong Zhu[2], Shenliang Chen[2]

[1]Shanghai National Engineering Research Center of Urban Water Resources Co., Ltd., Shanghai, 200082, P. R. China

[2]State Key Laboratory of Estuarine and Coastal Research, East China Normal University, Shanghai, 200241, P. R. China

[3]College of Environmental Science and Engineering, Tongji University, Shanghai, 200092, P. R. China

Corresponding author: Jianrong Zhu (jrzhu@sklec.ecnu.edu.cn)

Key points:

- Tidal forcing enhances the subtidal downstream transport of water and sediments off the Yellow River mouth into the Laizhou Bay
- The wave-induced bottom shear stress plays a more important role in sediment resuspension than tide-induced bottom shear stress in winter
- Tidal mixing strengthens the upward diffusion of bottom suspended sediments

Abstract

The fresh water and sediments transport from the Yellow River mouth downstream along the coast into the Laizhou Bay under the northeasterly wind in winter. The sediment transport is convergence in the river mouth, divergence in the downstream area, and convergence in the north of Laizhou Bay. Tide and wave are the two main forcings affecting the transport of water and sediments off river mouths. For the high-turbidity Yellow River mouth and the adjacent sea, tidal forcing enhances the subtidal downstream transport of water and sediments off the river mouth into the Laizhou Bay, whereas wave forcing has little effect on the advection of water and sediments. The sediment resuspension is controlled by the bottom shear stress induced by tide and wave. The tide-induced bottom shear stress is higher in the north of Laizhou Bay and south of Bohai Bay due to the stronger bottom tidal current. The wave-induced bottom shear stress plays a more important role in sediment resuspension, which is higher in the nearshore region along the Yellow River Delta away from the coast to some extent on account of the maximum near-bottom wave orbital velocity. Tidal mixing strengthens the upward diffusion of bottom suspended sediments. Without tidal forcing, the decreased bottom shear stress suspends less sediment above bed. On the other hand, the enhanced stratification hinders the upward diffusion of the bottom sediment due to the lack of tidal mixing, resulting in higher suspended sediment concentration (SSC) in the bottom layer in the offshore region.

Key words: Water and sediment transport; suspended sediment; bottom shear stress; tide; wave

Plain Language Summary

The Yellow River is well-known for its high sediment concentration, resulting in a rapid erosion-accretion pattern in the Yellow River Delta. Remote sensing images show that high-turbidity water appears from the Yellow River mouth to the north of Laizhou Bay, and in the south of Bohai Bay. The area is larger in winter and smaller in summer. The fresh water from the Yellow River mainly transports southward into Laizhou Bay. Most of the river sediment deposits in the river mouth, while part of it is carried southward. Wind waves induces high turbidity in the coastal sea in winter. Numerical experiment results show that tidal forcing also plays a role in sediment resuspension and more importantly in water and sediment transport in the horizontal direction. In addition, the stratification in the water column is highly controlled by tidal mixing rather than wave mixing. This paper discusses the effect of tide and wave on the transport of water and sediment in the Yellow River mouth and adjacent sea in winter. Three numerical experiments with or without tide/wave are implemented and cross-section fluxes are calculated to demonstrate the direction and magnitude of the transport.

1. Introduction

The Bohai Sea is a shallow semi-enclosed marginal sea in West Pacific, and the only inner Sea in China (Figure 1). The Bohai Sea receives about 1.5×10^{10} m^3 freshwater and 6.9×10^8 t sediment annually from the Yellow River (Cheng et al., 2021a), the second largest river in China, which is famous for its high sediment concentration. The water and sediment discharge of the Yellow River varies seasonally. Due to the frequent rainfall in flood season (July to October), the discharge is higher in flood season and lower in dry season (Wang et al., 2007; Yu et al., 2013). About 30 ~ 40% sediment from the Yellow River trapped in the river mouth, forming the Yellow River Delta (Li et al., 1998a), which is well-known for its rapid erosion-deposition variation (Cui and Li, 2011). The Yellow River Delta and adjacent sea are of great socio-economic importance and rich in biological resources, which are highly influenced by the water and sediment transport of the Yellow River (Kong et al., 2015).

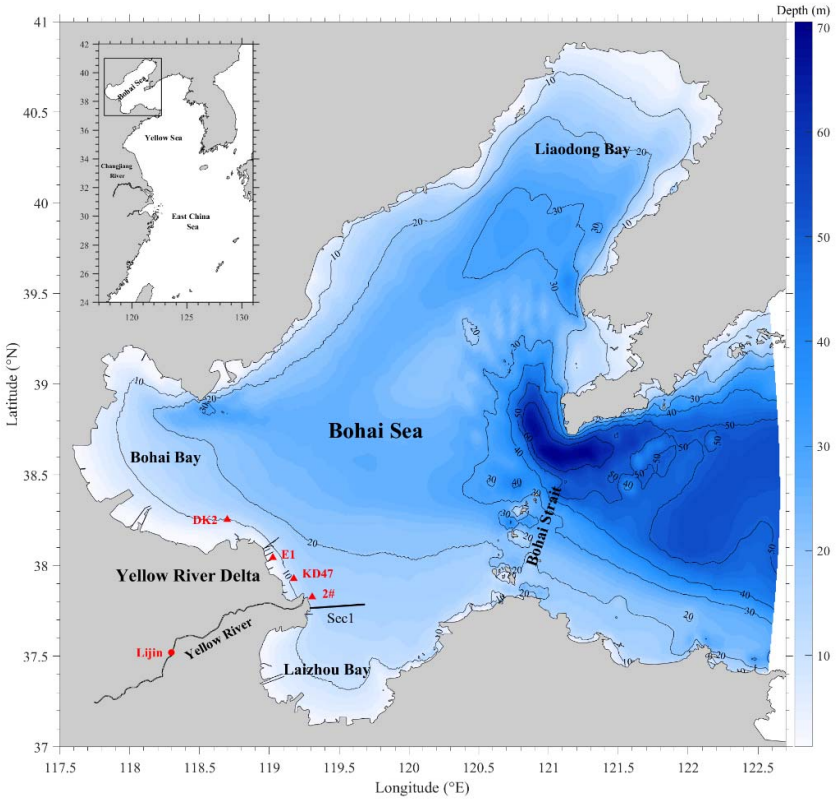

Figure 1. Topography of the Bohai Sea. The black contours are water depth, unit m; the red solid circle denotes the location of the Lijin hydrologic station; and the red triangles signify the locations of anchored ship measurement sites.

The transport of water and sediments off river mouth is influenced by river discharge, tide, wave, topography, temperature, salinity, etc (Fettweis et al., 1998). Among those factors, data showed that wave and tidal currents are the two dominant ones affecting the transport of water and sediment, and further influence the suspended sediment concentration (SSC) in the river mouth (Chen, 2001). Wolanski et al. (1995) studied the sediment transport in the Fly River estuary and found that at least three-quarters of the sediment from the river settled in the estuary. Numerical results showed that the turbidity maximum is caused by the simultaneous influence of

87 the baroclinic circulation and the tidal pumping, resulting in the turbidity maximum in
88 the Fly River estuary existing only at spring tides. The vertical stratification caused by
89 the residual baroclinic circulation driven by the along-channel density gradient plays
90 an important role in trapping sediment in the turbidity maximum. As a result, the
91 turbidity maximum is often located at the upstream limit of the salt intrusion (Lin and
92 Kuo, 2001).

93 The sediment transport shows flood and ebb variability. The eddy viscosity is
94 higher during flood tide and lower during ebb tide in a partially mixed estuarine
95 channel. This strong tidal asymmetry in turbulent mixing due to tidal straining
96 induces more sediment resuspended during flood tide. As a result, there is an
97 up-estuary pumping of sediment despite a net down-estuary advective flux (Geyer,
98 1993; Scully and Friedrichs, 2003; 2007; Simpson et al., 1990). For fine cohesive
99 sediments, the stronger turbulent mixing during flood tide plays a role in break-up of
100 aggregated flocs, resulting in the change of settling velocity (Traykovski et al., 2004;
101 van Leussen, 1988).

102 There exists a shear front zone off the Yellow River mouth, where sediment is
103 accumulated as a result of low velocity between flood and ebb (Li et al., 2001). Most
104 of the river-laden sediment deposit inside the shear front with a high accumulation
105 rate, while erosion is dominant outside the shear front due to the lack of sediment
106 supply (Wang et al., 2007). Qin and Li (1983) found that about 80% of the sediment
107 deposited in the region less than 30 km away from the Yellow River mouth. Only less
108 than 2% of the sediment can transport to the Yellow Sea through Bohai Strait (Martin

et al., 1993).

Surface waves are assumed to be the major cause of sediment resuspension by influencing the bottom shear stress in shallow waters, especially during significant wind events (Luettich et al., 1990). Wave induced sediment resuspension is 3 – 5 times higher than tide induced resuspension in upper Chesapeake Bay (Sanford, 1994). The SSC in the bottom layer increases with both wave height and wave bottom orbital velocity (Liu and Cai, 2019). Sediments are resuspended mostly during flood tides that followed wave events during low water in the shallow waters of South San Francisco Bay. However, the strong sediment transport is a result of the nonlinear interaction of wind waves and the tidal currents (Brand et al., 2010).

The tidal regime off the Yellow River mouth is irregular semidiurnal tides and the average tidal range is 0.6-1.0 m (Pang and Si, 1979). There is an amphidromic points of M_2 tidal constituent near Dongying station, north of the current Yellow River mouth. The tidal currents are rectilinear along the Yellow River Delta and rotary in the central Bohai Sea (Fan and Huang, 2005; Li et al., 1998b). The flood current usually flows SSE, while the ebb current directs NNW around the Yellow River mouth (Fan et al., 2006). The prevailing wind in Bohai Sea is northerly wind with a speed of 5 ~ 10 m/s in winter and southerly wind with a lower speed of 1 ~ 3 m/s in summer influenced by the East Asian Monsoon (Bian et al., 2013). As a result, the wave is stronger in winter and weaker in summer. The significant wave height and wave period are higher in the central Bohai Sea, and decrease shoreward (Lv et al., 2014).

Previous studies have done a lot of work explaining the dynamics of water and

sediment transport in the river mouths. However, the dynamic mechanism of water and sediment transport in the Yellow River mouth and adjacent seas is little-known, especially the responses to tide and wave. This paper explores the influence of tide and wave to the transport of water and sediment in the Yellow River mouth and the adjacent sea in winter, by using a 3-D high-resolution numerical model. The detailed model description and validation are presented in section 2. The results of numerical experiments and the dynamics of water and sediment transport are analyzed in section 3. The responses of water and sediment transport to tide and wave are discussed in section 4. Finally, the conclusions are presented in section 5.

2. Methods

2.1. Numerical model

2.1.1. Hydrodynamic model

The 3-D hydrodynamic numerical model is based on the ECOM-si (Estuarine, Coastal and Ocean Model semi-implicit) (Blumberg, 1994), which is developed from Princeton Ocean Model (POM) (Blumberg and Mellor, 1987), and later improved by Zhu (2003) and Chen et al. (2004). The model adopts the “Arakawa C” grid difference scheme (Arakawa and Lamb, 1977) and non-orthogonal curvilinear grids in the horizontal direction. In the vertical direction, the model uses σ coordinate system. The vertical eddy viscosity and diffusivity coefficients are calculated by the modified Mellor and Yamada level 2.5 turbulence closure scheme (Mellor and Yamada, 1974;

1982). The horizontal mixing processes are computed by the parameterization of Smagorinsky's scheme (Smagorinsky, 1963). The transport equations are solved by the third-order spatial interpolation at a moderate temporal resolution coupled with a TVD limiter (HSIMT-TVD) advection scheme to prevent numerical oscillations and reduce numerical dissipation (Wu and Zhu, 2010).

The model domain covered the entire Bohai Sea and part of the north Yellow Sea (Figure 2). The model grid consisted of 381 × 335 cells in the horizontal dimension. The vertical direction was divided by ten σ layers. The model time step was variable based on the CFL (Courant, Friedrichs and Lewyt) criterion instead of using a constant value. A wet/dry scheme describing the intertidal flat with a critical depth of 0.2 m was included in the model. The upstream river boundary was set at Lijin hydrological station and *in situ* water and sediment discharge were set as boundary condition. The open sea boundary in the north Yellow Sea was driven by sixteen astronomical tidal constituents: M_2, S_2, N_2, K_2, K_1, O_1, P_1, Q_1, MU_2, NU_2, T_2, L_2, $2N_2$, J_1, M_1, and OO_1, which were derived from the NaoTide dataset (http://www.miz.nao.ac.jp/). The sea surface wind field was from the European Center for Medium-Range Weather Forecast (ECMWF) reanalysis dataset with a spatial resolution of 0.125° × 0.125° and a temporal resolution of 6 h. The wave boundary conditions were calculated by the Simulating Waves Nearshore (SWAN) model.

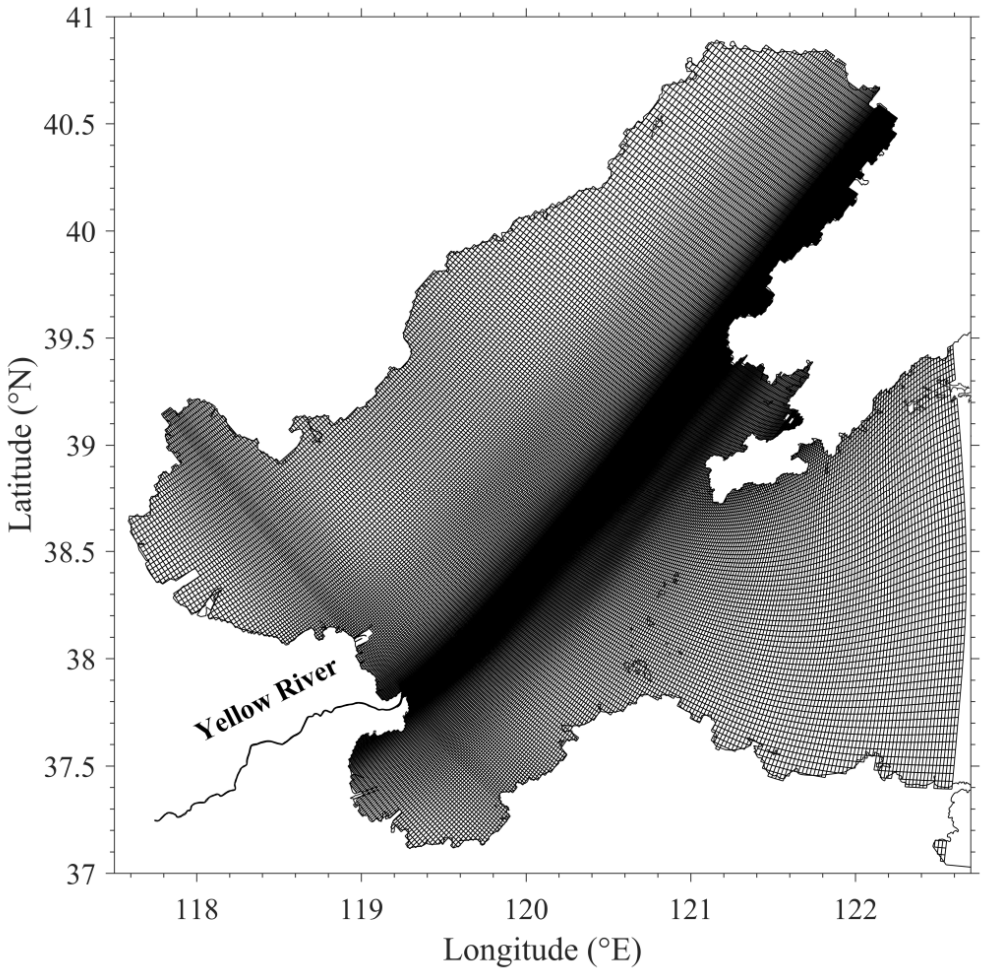

Figure 2. Model domain and grids

2.1.2. Sediment module

The sediment transport equation in the horizontal non-orthogonal curvilinear and vertical σ coordinate system can be written as

$$\frac{\partial \mathrm{DJC_{sed}}}{\partial \mathrm{t}} + \frac{\partial \mathrm{DJ\hat{U}C_{sed}}}{\partial \xi} + \frac{\partial \mathrm{DJ\hat{V}C_{sed}}}{\partial \eta} + \frac{\partial \mathrm{J}(\omega - \omega_{\mathrm{sed}})\mathrm{C_{sed}}}{\partial \sigma} = \frac{1}{\mathrm{D}}\frac{\partial}{\partial \sigma}\left(\mathrm{K_h}\frac{\partial \mathrm{JC_{sed}}}{\partial \sigma}\right) + \mathrm{DJF_{sed}} \quad (1)$$

where C_{sed} is SSC. ω_{sed} is sediment settling velocity, which is calculated as follows (Mehta and McAnally, 2008):

$$\omega_{sed} = \begin{cases} \omega_0 & C_{sed} \le C_{sed0} \\ \dfrac{m_1 {C_{sed}}^{n_1}}{\left({C_{sed}}^2 + {m_2}^2\right)^{n_2}} & C_{sed} > C_{sed0} \end{cases} \quad (2)$$

C_{sed0} is the critical sediment concentration for flocculation. According to Huang et al. (1980), $C_{sed0} = 0.2\ \mathrm{kg \cdot m^{-3}}$. The empirical coefficients m_1, n_1, m_2 and n_2 are set as 0.012, 2.2, 1.7 and 2.8. ω_0 is the free settling velocity.

The SSC initial condition is set as a homogeneous constant value. Ignoring the surface sediment flux, the sea surface boundary is calculated as:

$$\left(\omega_{sed} C_{sed} + \frac{K_v}{D}\frac{\partial C_{sed}}{\partial \sigma}\right)\Big|_{\sigma=0} = 0 \quad (3)$$

the sea bottom boundary is calculated as:

$$\left(\omega_{sed} C_{sed} + \frac{K_v}{D}\frac{\partial C_{sed}}{\partial \sigma}\right)\Big|_{\sigma=-1} = q_{dep} - q_{ero} \quad (4)$$

where q_{dep} and q_{ero} are the bottom sediment flux due to deposition and erosion, respectively, which can be calculated as follows (Cao and Wang, 1994):

$$q_{dep} = \begin{cases} 0, & \tau_b > \tau_d \\ \alpha' \omega_{sed} C_{sed}\left(1 - \dfrac{\tau_b}{\tau_d}\right), & \tau_b \le \tau_d \end{cases} \quad (5)$$

$$q_{ero} = \begin{cases} 0, & \tau_b < \tau_e \\ M\left(\dfrac{\tau_b}{\tau_e} - 1\right), & \tau_b \ge \tau_e \end{cases} \quad (6)$$

where τ_b is the simulated bottom shear stress. τ_e and τ_d are the critical shear stresses for erosion and deposition, respectively. α' is the deposition coefficient, which is generally set as 0.67~0.84; M is the erosion coefficient, which generally ranges from 1×10^{-5}~4×10^{-3} $\mathrm{kg \cdot m^{-2} \cdot s^{-1}}$.

The bottom shear stress under the influence of wave-current interaction is expressed as (Liang et al., 2008):

$$\tau_b = |\tau_{wm} + \tau_c|$$
$$= \sqrt{\tau_{wm} + \tau_c|\cos\Phi_{wc}|^2 + \tau_c \sin\Phi_{wc}{}^2} \quad (7)$$
$$= \tau_{wm}\sqrt{1 + 2\frac{\tau_c}{\tau_{wm}}|\cos\Phi_{wc}| + \left(\frac{\tau_c}{\tau_{wm}}\right)^2}$$

where τ_{wm} is the maximum wave bed shear stress. τ_c is the current shear stress. Φ_{wc} is the angle between wave propagation and the current.

The algorithm of wave bed shear stress is:

$$\tau_{wm} = \frac{1}{2}\rho f_{cw} u_{bm}^2 \quad (8)$$

where ρ is the water density. f_{cw} is the wave fiction factor, which can be evaluated with the empirical relations according to Signell et al. (1990). u_{bm} is the maximum near-bottom wave orbital velocity, which can be calculated as:

$$u_{bm} = \frac{0.5H\omega}{\sinh kh} \quad (9)$$

where k is the wave number. h is the water depth. $H = H_{rms} = H_s/\sqrt{2}$; $\omega = 2\pi/T$. H_s is the significant wave height. T is the significant wave period.

The current shear stress τ_c is related to bottom current velocity u_c:

$$\tau_c = \rho C_D u_c^2 \quad (10)$$

where C_D is the bottom drag coefficient under the influence of wave-current interaction, which is solved by an iterative procedure. Additional details about the calculation procedure can be found in Liang et al. (2008).

The critical shear stress is an important parameter to calculate the bottom sediment flux. The equation of Dou (Dou, 1999) considered the influence of sediment diameter and water depth to the sediment viscosity, which is suitable for areas with significant water depth variance. First, we collected the distribution of median particle

diameter D_{50} and water content W of surface bed sediment in the Bohai Sea. And then, the critical shear stress for erosion τ_e is calculated by the equation of Dou:

$$\tau_e = k^2 \rho_w \left(\frac{d'}{d^*}\right)^{1/3} \left(3.6\frac{\rho_s - \rho_w}{\rho_w} g D_{50} + \left(\frac{\gamma_0}{\gamma_0^*}\right)^{5/2} \left(\frac{\varepsilon_0 + gh\delta(\delta/D_{50})^{1/2}}{D_{50}}\right)\right) \quad (11)$$

generally, the parameter k is set as 0.128. Water density $\rho_w = 1025$ kg/m^3. Sediment density $\rho_s = 2650$ kg/m^3. ε_0 is the viscosity parameter, which is usually set as 1.75. δ is the thickness of pellicular water, which is measured as 2.31×10^{-5} cm in the laboratory. $d' = 0.5$ mm is the height of roughness. $d^* = 10$ mm. γ_0 is the sediment dry density, whereas γ_0^* is the stable dry density, the ratio of which represents the compaction rate of bed sediment. The value of γ_0^* refers to Han (1997). The sediment dry density is calculated as:

$$\gamma_0 = \frac{\rho_w}{W + \frac{\rho_w}{\rho_s}} \quad (12)$$

The component of bed sediment is variable in the Yellow River mouth and the adjacent sea, including grit, fine sand, silt, clay, etc. The sediment diameter varies between 0.005 ~ 0.08 mm (Sun, 2013). The water content of bed sediment is lower (50 % ~ 60 %) in the north side of the current Yellow River mouth and higher (about 80 %) in the south side. According to the sediment diameter, water content and water depth, the calculated critical shear stress for erosion in the Bohai Sea by the equation of Dou is shown in Figure 3. The critical shear stress for erosion along the Yellow River Delta is lower than 0.5 N/m^2 ; while in the northeast side of the current Yellow River mouth, the critical shear stress for erosion is about 0.8 N/m^2. The critical shear

stress in some areas of north of Laizhou Bay is higher because these areas are dominated by fine cohesive sediment. The critical shear stress for deposition τ_d is calculated as (Cao and Wang, 1994):

$$\tau_d = \frac{4}{9}\tau_e \quad (13)$$

Based on the calculated critical shear stress for erosion and deposition, the model was calibrated and validated using measured and remote sensing retrieval SSC data to get a better distribution of critical shear stress suitable for the current Yellow River mouth and adjacent sea.

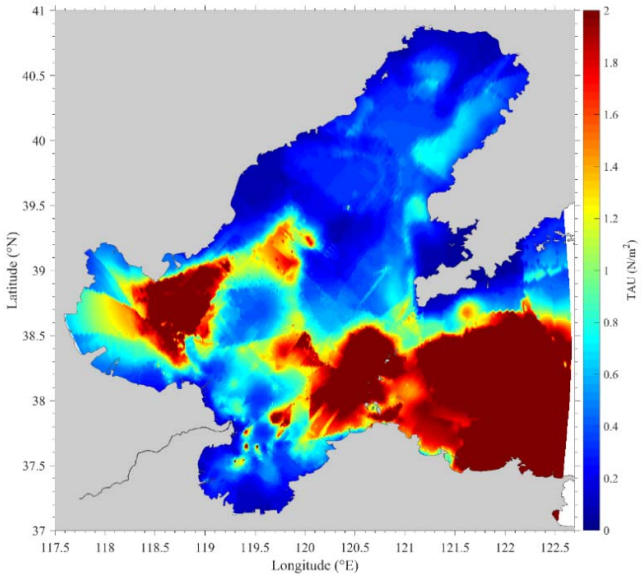

Figure 3. Critical shear stress of bed sediment for erosion in the Bohai Sea

2.2. Model validation

The model has been well calibrated and verified many times for elevation, current velocity and salinity in previous studies (Cheng et al., 2021a; 2021b). This study further validated the model with current, salinity, SSC and wave for SWAN model. The following three skill assessments were used to quantify the validations:

correlation coefficient (CC), root mean square error (RMSE), and skill score (SS) (Murphy, 1988; Ralston et al., 2010):

$$\mathrm{CC} = \frac{\sum_{i=1}^{N}(X_{mod}-\bar{X}_{mod})(X_{obs}-\bar{X}_{obs})}{(\sum_{i=1}^{N}(X_{mod}-\bar{X}_{mod})^2 \sum_{i=1}^{N}(X_{obs}-\bar{X}_{obs})^2)^{1/2}} \quad (14)$$

$$\mathrm{RMSE} = (\sum_{i=1}^{N} \frac{(X_{mod}-X_{obs})^2}{N})^{1/2} \quad (15)$$

$$\mathrm{SS} = 1 - \frac{\sum_{i=1}^{N}(X_{mod}-X_{obs})^2}{\sum_{i=1}^{N}(X_{obs}-\bar{X}_{obs})^2} \quad (16)$$

where X is the variable of interest and $\bar{X}$ is the time-averaged value. The agreement between the modeled results and observed results is assessed as follows by SS: >0.65 excellent; 0.65-0.5 very good; 0.5-0.2 good; and <0.2 poor (Liu et al., 2009; Maréchal, 2004).

2.2.1. Current, salinity and SSC

We used the *in situ* water velocity, salinity and SSC data at the anchored ship stations (labeled in Figure 1) to validate the model. Site DK2 was measured from 29 to 30 August 2018; site E1 was measured from 11 to 12 October 2009; site 2# was measured from 6 to 7 August 2017. The mean water depths at sites DK2, E1 and 2# were 9.3, 6.91 and 5.7 m, respectively.

The comparisons between the observed data and the simulated results are shown in Figure 4. At the measured site DK2, the current was rectilinear, the flood current velocity was almost the same as the ebb current velocity, and the bottom velocity was smaller than the surface velocity due to bottom friction. The salinity was approximately 30.5 at the surface layer and 30.5 at the bottom layer with almost little temporal variation. The SSC varied with tide, with maximum value 0.15 kg/m^3 at

surface and 0.2 kg/m^3 at bottom. At the measured site E1, the water velocity was smaller than DK2 and 2# due to the artificial dams nearby. The maximum surface water velocity was only 0.6 m/s. The surface salinity was approximately 27.5 and the bottom salinity was about 28 with a little temporal variation. The maximum SSC was 0.12 kg/m^3 at the surface layer and 0.17 kg/m^3 at the bottom layer with a downtrend. At the measured site 2#, the maximum water velocity was 0.9 m/s at the surface layer and 0.6 m/s at the bottom layer. The salinity had a semidiurnal variation with a minimum salinity of 5.1 and maximum salinity of 29.5 at the surface layer. The maximum SSC was 0.25 kg/m^3 at the surface layer and 0.26 kg/m^3 at the bottom layer.

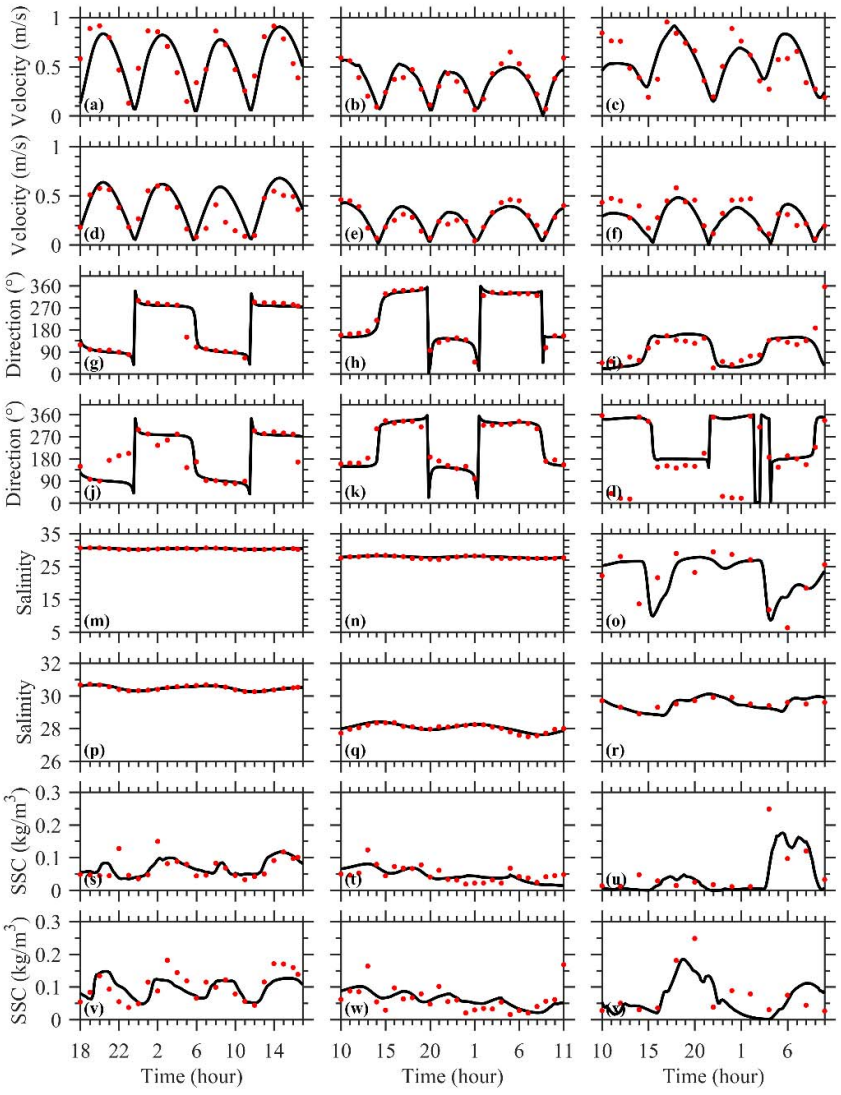

Figure 4. Comparisons between the observed data (red dots) and the simulated results (black line). The left column represents Site DK2, the middle column represents Site E1 and the right column represents Site 2#. (a, b, c): surface velocity; (d, e, f): bottom velocity; (g, h, i): surface direction; (j, k, l): bottom direction; (m, n, o): surface salinity; (p, q, r): bottom salinity; (s, t, u): surface SSC; and (v, w, x): bottom SSC.

The CC, RMSE and SS for comparison of modeled and observed water velocity and salinity at the measured sites are shown in Table 1. The mean CC, RMSE and SS were 0.79, 0.14 m/s, and 0.57 for the surface water velocity, respectively, 0.84, 0.09

m/s, and 0.61 for the bottom water velocity, respectively, and 0.82, 0.12 m/s, and 0.59 for the vertically averaged water velocity, respectively. The mean CC, RMSE and SS were 0.76, 2.04, and 0.45 for the surface salinity, 0.88, 0.13, and 0.64 for the bottom salinity, respectively, and 0.82, 1.09, and 0.55 for the vertically averaged salinity, respectively. The mean CC, RMSE and SS were 0.61, 0.04 kg/m^3, and 0.31 for the surface SSC, 0.62, 0.04 kg/m^3, and 0.35 for the bottom SSC, respectively, and 0.62, 0.04 kg/m^3, and 0.33 for the vertically averaged SSC, respectively. Generally, the model reproduced the processes of the water current, salinity and SSC well and can be used to study the hydrodynamics and sediment transport in the Bohai Sea.

Table 1. CC, RMSE, and SS for comparison of modeled and observed water velocity, salinity and SSC at the measured stations.

Station	DK2			E1			2#		
skill assessment	CC	RMSE	SS	CC	RMSE	SS	CC	RMSE	SS
Surface velocity (m^3/s)	0.71	0.19	0.37	0.91	0.07	0.82	0.74	0.16	0.53
Bottom velocity (m^3/s)	0.83	0.13	0.50	0.90	0.05	0.82	0.80	0.10	0.50
Surface salinity	0.87	0.11	0.64	0.78	0.30	0.36	0.64	5.70	0.36
Bottom salinity	0.97	0.04	0.93	0.86	0.12	0.72	0.80	0.22	0.28
Surface SSC (kg/m^3)	0.61	0.03	0.34	0.60	0.02	0.30	0.61	0.06	0.28
Bottom SSC (kg/m^3)	0.59	0.04	0.32	0.64	0.03	0.38	0.62	0.05	0.36

2.2.2. Remote sensing retrieval and validation

The sea surface SSC was validated using remote sensing retrieval in winter and summer of Landsat 8 OLI (Operational Land Imager imagery), which was downloaded from USGS (http://glovis.usgs.gov/). The remote sensing image was captured in March and August 2018 (Figure 5). Studies show that the spectral reflectance of 700-900 nm in the image is more sensitive to the variation of sea surface SSC (Doxaran et al., 2002). The green or blue band combined with near-infrared band are more suitable for the retrieval of high turbidity water near the Yellow River mouth (Long and Pavelsky, 2013). Therefore, the SSC retrieval formula of Zhan et al. (2017) was adopted, which is given by:

$$\mathrm{SSC} = 1622.6X^3 - 3518.7X^2 + 3180.8X - 544.7 \quad (17)$$

where the unit of SSC is mg/L; $X = R_{rs}(820)/R_{rs}(490)$, $R_{rs}(820)$ and $R_{rs}(490)$ are the sea surface spectral reflectance of 820 nm and 490 nm, respectively.

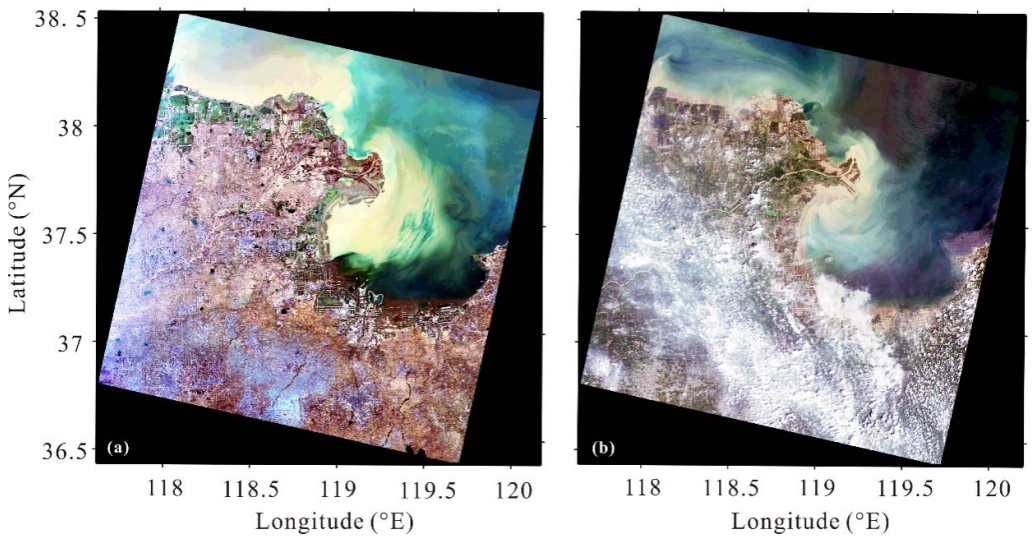

Figure 5. Remote sensing images of Landsat 8 OLI in the sea near the Yellow River mouth in March (a) and August (b) 2018.

The remote sensing retrieval and validation of sea surface SSC is shown in Figure 6. The sea surface SSC is higher in winter and lower in summer. In winter, the sea surface SSC is higher near the Yellow River mouth, north of Laizhou Bay and south of Bohai Bay. The retrieval SSC corresponds to the remote image. In summer, the sea surface SSC is higher in the Yellow River mouth and north of Laizhou Bay, with the highest value lower than 1 kg/m^3. The simulated sea surface SSC is close to the retrieval result. The simulated high SSC areas correspond to the retrieval, but the magnitude of SSC is a little higher than the retrieval SSC. Generally, the remote sensing retrieval and model validation results are well. Therefore, the model can be used to study the SSC variation in the Yellow River mouth and adjacent sea.

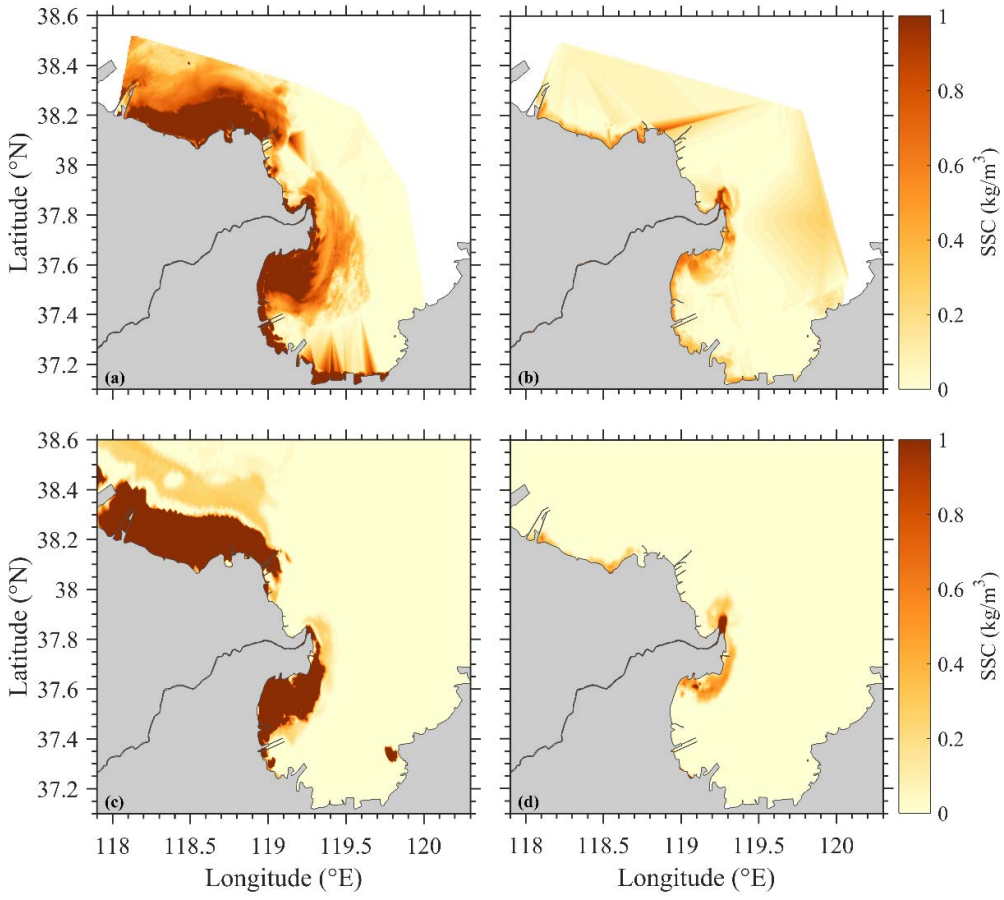

Figure 6. Comparisons between the remote sensing retrievals of sea surface SSC from Landsat 8 images (a, b) and model results (c, d) in March (a, c) and August (b, d) 2018.

2.2.3. Wave

The wave parameters are simulated by the SWAN model. The model is validated using measured significant wave height and period of 9-22 November 2012 in site KD47 (labeled in Figure 1) (data from Wang (2014)). As shown in Figure 7, the variation of simulated significant wave height and period correspond to the measured data. However, the simulated crest of significant wave height is lower than measured data, which might be the result of low time resolution of wind data. Generally, the SWAN model simulated the wave parameters well. And therefore, it is able to provide the wave boundary condition in the ECOM-si model.

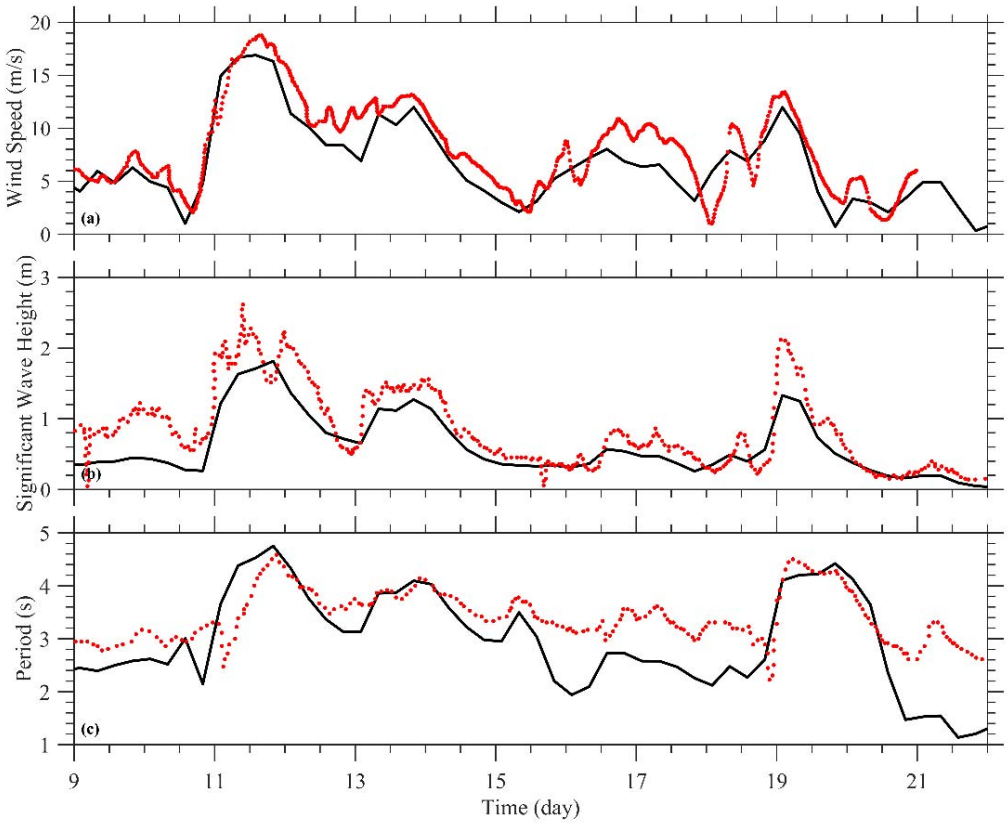

Figure 7. The wind speed (a), significant wave height (b), and period (c) from 9 to 22 November 2012 at Site KD47 (the line in (a) denotes ECMWF data, the lines in (b) and (c) denote SWAN model result, and the points in (a), (b), and (c) denote observed data).

2.3. Numerical experiment settings

Three numerical experiments were set to study the water and sediment transport off the Yellow River mouth in winter and the response to tide and wave (Table 2). Exp 0 is the control experiment, which considered river discharge, tide, wave, etc. Exp 1 excluded the influence of tide in order to study the effect of tide on the water and sediment transport. Exp 2 excluded the influence of wave in order to study the effect of wave by comparing with Exp 0. The model ran from January to December, and the

subtidal results during spring tide in December were analyzed. The river discharge is the monthly-mean data recorded in Lijin hydrologic station. The wind data is from ECMWF with a time resolution of 6 h. The wave boundary condition is the simulated results of SWAN model. The residual sediment flux is used to represent the sediment transport in the shallow sea with tidal rise and fall. This flux is calculated as follows:

$$\overrightarrow{F_C} = \frac{1}{T}\int_0^T \int_{h_1}^{h_2} \vec{V} \cdot C_{sed} dz dt \quad (18)$$

where T is the averaged time of 6 tidal periods, which is approximately 3 days; h_2 and h_1 are the top and bottom depths of the water layer, respectively; C_{sed} is SSC; and $\vec{V}$ is the horizontal velocity.

Table 2. Setup of the different experiments

Experiment	Tide	Wave
0	√	√
1	×	√
2	√	×

The convergence and divergence of sediment transport (condiv) is used to reflect the sediment transport condition. The formula is given by:

$$\mathrm{condiv} = \frac{\partial u C_{sed}}{\partial x} + \frac{\partial v C_{sed}}{\partial y} \quad (19)$$

where x and y are the east and north direction respectively; u and v are the velocity in the east and north direction. The variation of SSC in the water column induced by the horizontal sediment transport is calculated by integrating the horizontal sediment transport term vertically. The convergence of sediment transport means the SSC increased locally, while divergence means the SSC decreased locally.

3. Result

The prevailing wind above the Bohai Sea is northeasterly during spring tide in December 2012, with the values of 5 ~ 7 m/s. The northeasterly wind induced a northwestward Ekman transport. As a result, the residual water fluxes in the Bohai Sea in the surface layer are mostly westward/northwestward (Figure 8a). The fresh water off the Yellow River flows downstream (the direction in which a Kelvin wave propagates) into the Laizhou Bay, resulting in a lowest salinity value of about 25 in Laizhou Bay. The residual water fluxes in Laizhou Bay are lower than 0.01 m^3/s due to the weak salinity gradient. The salinity gradient is higher to the east of Laizhou Bay, due to the stronger residual water flux from the coast to the northwest induced by the Ekman transport. The salinity distribution in the bottom layer is close to the surface layer as a result of the strong vertical mixing in winter (Figure 8b). The bottom salinity to the east of Laizhou Bay is higher than the surface layer, where the bottom residual water fluxes are southward across the salinity gradient induced by the baroclinic gradient force, with the values of 0.04 ~ 0.1 m^3/s. The bottom residual water fluxes in the central area of Bohai Sea are northeastward due to the compensational transport for water conservation with the values lower than 0.04 m^3/s. However, the water transports in the south of Bohai Bay and the head of Laizhou Bay are weak due to the homogeneous salinity distribution.

The strong wind in winter induces strong wave effect along the coast. As a result, the bottom shear stress induced by wave is higher in the shallow water along the coast of Yellow River Delta (Figure 9b). The bottom shear stress induced by tide is higher

in the north of Laizhou Bay and south of Bohai Bay due to the larger water velocities. The total bottom shear stress is strong along the coast of Yellow River Delta, with the maximum values in the north of Laizhou Bay and south of Bohai Bay. The total bottom shear stress suspends the bed sediment to the upper layer. As a result, the bottom SSC is higher than 2 kg/m^3 along the coast of Yellow River Delta, whereas the surface SSC is higher in the north of Laizhou Bay and south of Bohai Bay, which corresponds to the bottom shear stress induced by tide. The directions of residual water velocities are similar to the residual water fluxes (Figure 8c, d). The water from the Yellow River flows downstream along the coast, carrying the river sediment into Laizhou Bay. The residual water velocities are 0.05 ~ 0.15 m/s and the residual sediment fluxes are 0.15 ~ 0.2 kg/s in the surface layer to the downstream of the Yellow River mouth (Figure 8e). In the bottom layer, the residual water velocities and sediment fluxes are in the same direction as surface layer, but weaker than surface. Therefore, the sediment sources of this area are Yellow River and local bottom sediment resuspension. In the north side of the Yellow River mouth, the surface residual water velocities and sediment fluxes are upstream, but a lot weaker than the south of river mouth. Thereby, the surface SSC in the north side of the river mouth is lower than 0.5 kg/m^3. In the south of Bohai Bay, the water and sediment transports are westward. The residual water velocities are 0.02 ~ 0.05 m/s and the residual sediment fluxes are 0.05 ~ 0.3 kg/s. The SSC in the south of Bohai Bay is higher at bottom and lower at surface. However, the sediment transport is stronger at surface and weaker at bottom. The strong bottom shear stress in the south of Bohai Bay and the far distance

from the river mouth suggest that the high SSC is mainly caused by local bottom sediment resuspension.

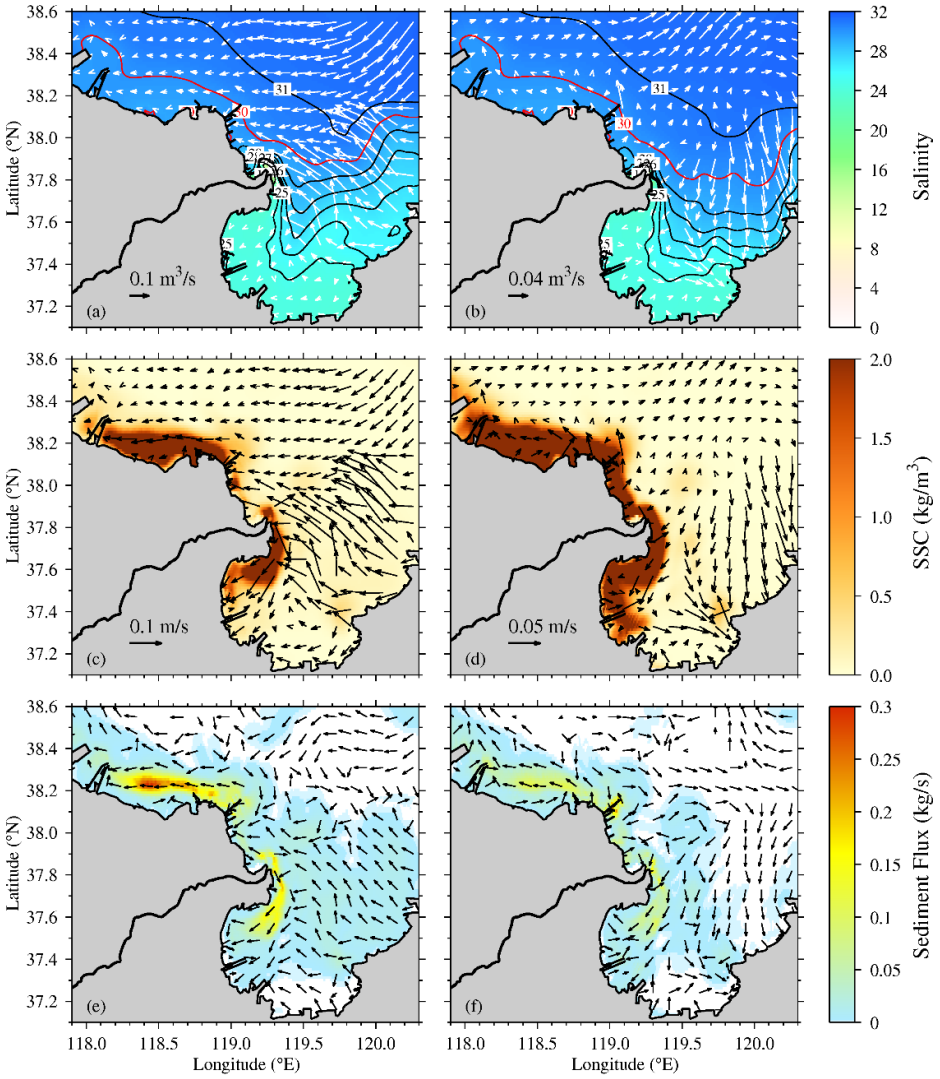

Figure 8. Distributions of residual unit width water flux and salinity (a, b), residual water velocity and SSC (c, d), residual unit width sediment flux (e, f) at surface layer (left panel) and bottom layer (right panel) during spring tide in December 2012 in Exp 0 (arrows only signify direction, color signify the value of residual sediment flux in e and f).

The sediment transport converges in the Yellow River mouth with sediment fluxes of about 0.1 g/m^2/s as a result of river sediment deposition (Figure 9d). There is

a divergence area on the east of the convergence area, which means that part of the sediment transport landward to the river mouth. The sediment transport is divergence to the downstream of the river mouth with sediment fluxes of about 0.08 g/m^2/s, whereas in the adjacent north of Laizhou Bay, the sediment transport converges with fluxes of 0 ~ 0.06 g/m^2/s. It is presumable that the sediment from the Yellow River transport downstream along the coast and mainly deposit in the north of Laizhou Bay. To the upstream of the Yellow River mouth, the sediment transport is divergence nearshore and convergence offshore, indicating that sediment transport from the coast to the sea. In the south of Bohai Bay, the sediment transport is divergence at the east side and convergence at the west side. The residual sediment fluxes are about 0.04 ~ 0.06 g/m^2/s. The sediment transport in the south of Bohai Bay is westward, which corresponds to the diagram of residual sediment flux (Figure 8e, f).

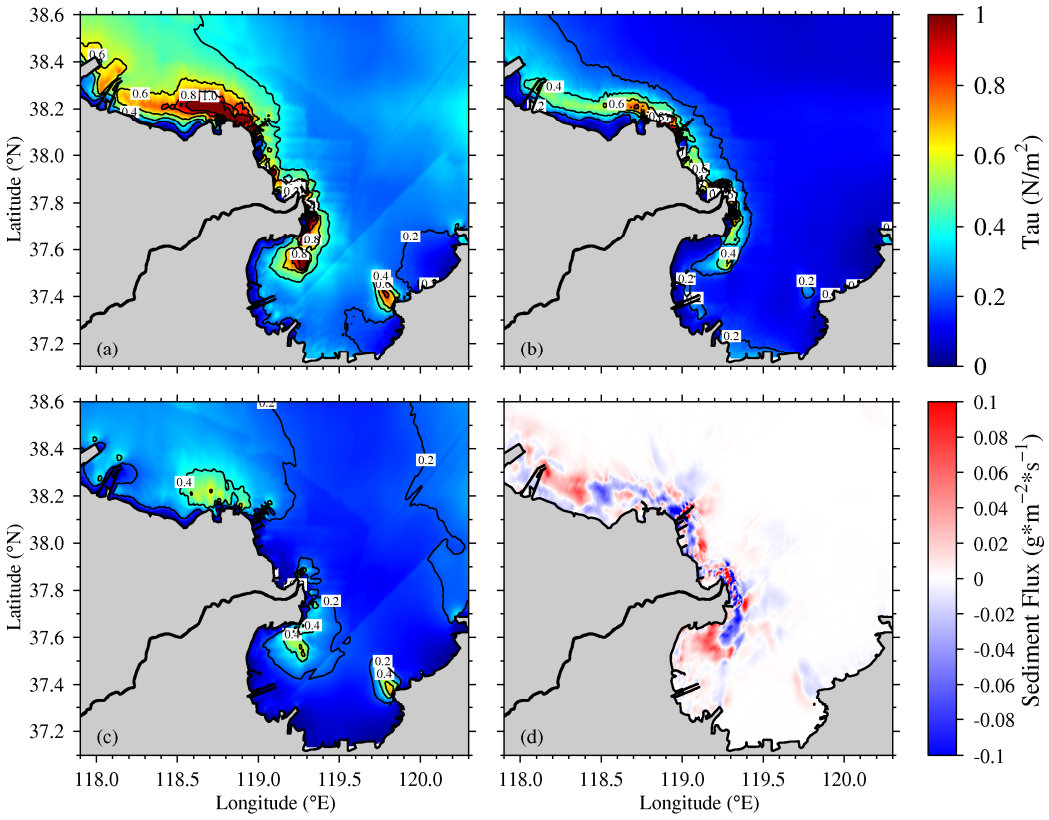

Figure 9. Distributions of total bottom shear stress (a), bottom shear stress induced by wave (b), bottom shear stress induced by tide (c), and sediment convergence and divergence (d) during spring tide in December 2012 in Exp 0 (positive value and red color indicate convergence, negative value and blue color indicate divergence in d).

Sec 1 is located at the south side of the Yellow River mouth (labelled in Figure 1). The residual water currents along Sec 1 are mainly landward in the surface layer driven by the westward Ekman transport induced by the northeasterly wind. The surface residual water velocities along Sec 1 are about 1 ~ 8 cm/s. In the bottom layer, the along-section residual water currents are also landward due to the baroclinic gradient force. However, the velocities are much smaller than surface layer, with values lower than 1 m/s. The strong landward surface currents induce an upwelling at about 28 km away from the coast and a downwelling at 10 km away from the coast,

which is suggested to be the result of the convergence and divergence of Ekman transport in the bottom boundary layer during the trapping of the river plume front (Chapman and Lentz, 1994; Cheng et al., 2021a; Wu and Wu, 2018). As for the cross-section currents, the residual water flows downstream within 8 km away from the coast with the velocities of larger than 6 cm/s. At the seaward side of Sec 1, the residual water flows upstream in the surface layer due to the Ekman transport and downstream in the bottom layer as compensational flow across the section. The maximum cross-section water velocities are higher than 6 cm/s at surface and lower than 4 cm/s at bottom.

The strong wind wave in winter induces strong vertical mixing in the shallow water. As a result, the salinity is well mixed at the nearshore side of Sec 1 (Figure 10b). Within 4 km away from the coast, the salinity in the surface layer is about 23 as a result of the fresh water flowing downstream across Sec 1. At the seaward side of the section, the salinity is stratified in the water column due to the downstream transport of saline water in the bottom layer induced by the baroclinic gradient force, with surface salinity lower than 29 and bottom salinity close to 30. The SSC profile indicates that high SSC area is located with 10 km away from the coast. The SSC in the water column is stratified within 5 km and mixed out of 5 km away from the coast. The maximum SSC along Sec 1 is about 5 kg/m^3 in the near-bed layer at about 1 ~ 3 km away from the coast, and decreasing upward to about 3 ~ 4 kg/m^3 in the surface layer. It is predictable that the nearshore high SSC is mainly derived from bottom sediment resuspension rather than along-shelf sediment transport.

456 The water flux and salinity flux across Sec 1 show similar temporal variation
457 (Figure 11a, b). The water and salt transport are mainly downstream in December
458 2012, especially in early of the month. During spring tide, the total water and salt flux
459 across Sec 1 are firstly upstream, and then turn to downstream, and once again divert
460 to upstream. The maximum water flux is about 0.8×10^4 m^3/s and the maximum salt
461 flux is about 200 kg/s, both in the downstream direction. However, the sediment flux
462 across Sec 1 is mainly in the downstream direction in December because the sediment
463 from Yellow River transport downstream across the section. During spring tide,
464 sediment transport downstream across Sec 1 with fluxes of about $0 \sim 1\times10^4$ kg/s.

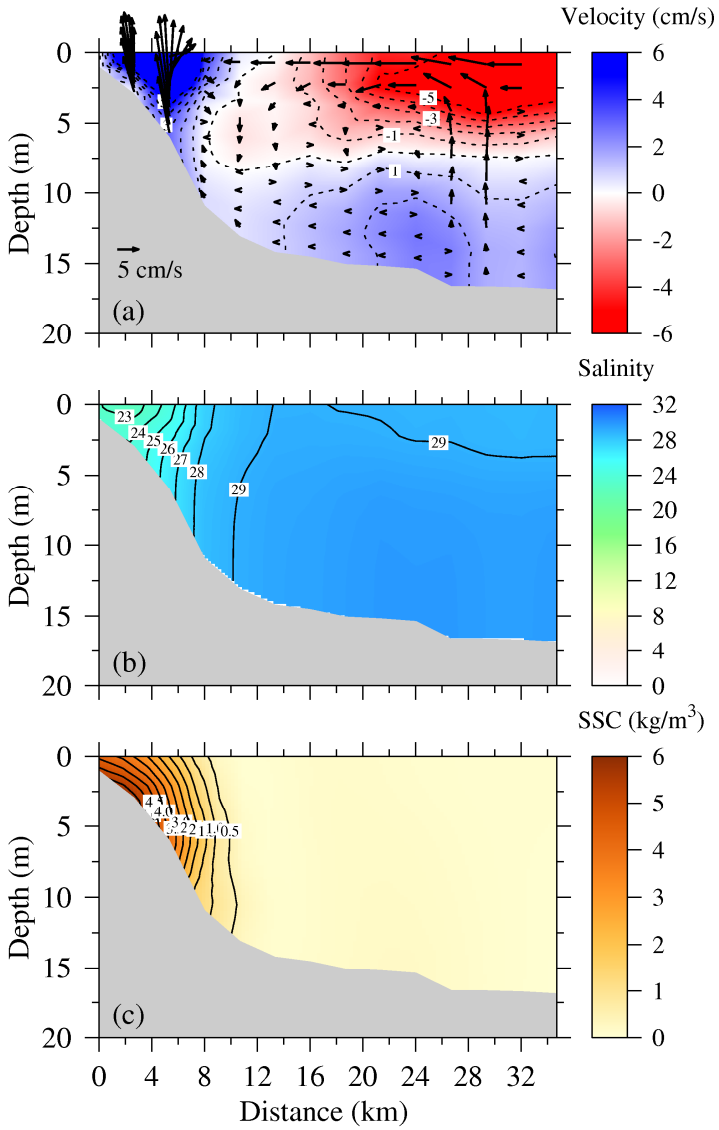

Figure 10. Vertical profile distributions of residual velocity (a), salinity (b) and SSC (c) along Sec 1 in Exp 0 during spring tide in December 2012 (arrows in (a) signify current vectors along section, and the contours signify current velocities perpendicular to the section. positive values indicate downstream current).

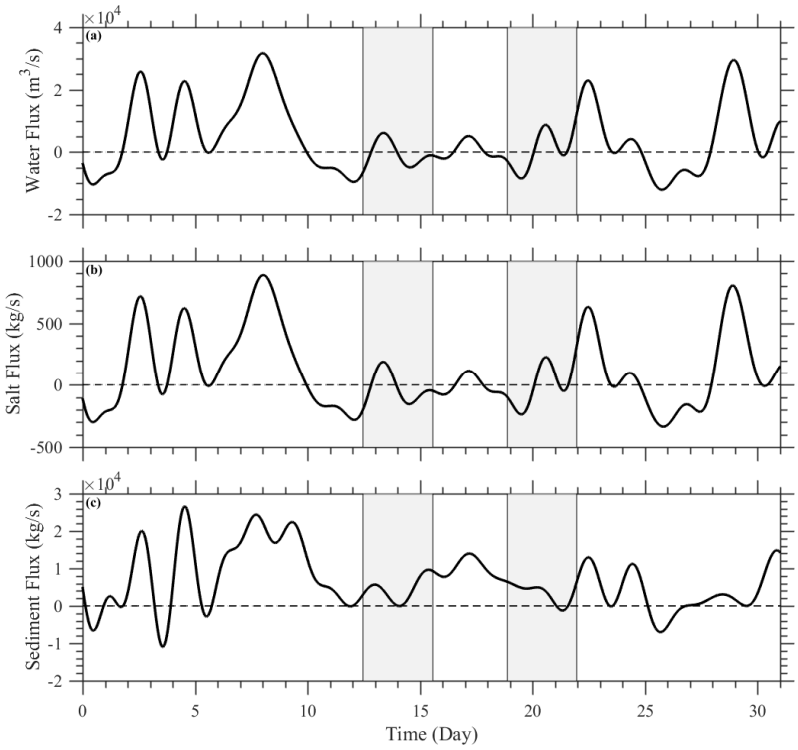

Figure 11. Temporal variations in water flux (a), salt flux (b) and sediment flux (c) across Sec 1 in December 2012 in Exp 0 (positive values indicate downstream transport; the left shadow indicates duration of spring tide, and the right shadow indicates duration of neap tide).

4. Discussion

4.1 The effect of tide on the transport of water and sediments

Exp 1 excluded tide from the driving forces and the results were compared with Exp 0. Without tidal forcing, the surface water currents are mainly driven by the northwestward Ekman transport induced by the northeasterly wind in winter. The residual water fluxes are larger in the central of Bohai Sea with values of 0.2 ~ 0.3 m^3/s, while smaller in the Laizhou Bay with values lower than 0.1 m^3/s due to the

special shoreline and topography. The low-salinity water transport upstream to some extent. However, the majority of low-salinity water penetrates downstream along the coast due to the geostrophic adjustment. In the bottom layer, the residual water fluxes are mainly downgradient of salinity induced by the baroclinic pressure gradient. The salinity is higher than surface layer and low-salinity water mostly transports downstream rather than upstream. The difference between Exp 0 and Exp 1 indicates the effect of tide. The tide induces downstream residual water fluxes along the coast of Yellow River Delta in the surface layer, and northward water fluxes in the central of Bohai Sea in the bottom layer. The salinity differences between Exp 0 and Exp 1 are positive in the surface layer near the Yellow River mouth especially in the north side, with values of 0 ~ 3, higher in the river mouth and decreasing offshore. This is induced by the combination effect of vertical mixing and more fresh water transporting downstream due to the tidal forcing. As a result, the salinity differences are negative in Laizhou Bay and extend northeast along the coast in both surface layer and bottom layer due to the shallow depth in Laizhou Bay (Figure 12c, d).

Without tidal forcing, the SSC decreases a lot in the surface layer, especially in the south of Bohai Bay and to the downstream of Yellow River mouth (Figure 12g). The maximum SSC in the surface layer is about 1.5 kg/m^3 in the river mouth. And in other areas along the Yellow River Delta with suspended sediments in the surface layer, the SSCs are about 0 ~ 1 kg/m^3. The bottom shear stress induced by wave remains unchanged, whereas the bottom shear stress induced by tide decreases about 0 ~ 0.5 N/m^2 in the south side of the Yellow River mouth, the east head of Laizhou

Bay, and the south of Bohai Bay (Figure 13). The bottom shear stress induced by tide is lower than 0.2 N/m^2, as a result, the total bottom shear stress is 0 ~ 1 N/m^2 along the Yellow River Delta mainly induced by wave. The lower bottom shear stress resuspends less sediment above bed. In the bottom layer, the SSCs are higher than 2 kg/m^3 along the Yellow River Delta. Compared with Exp 0, the bottom SSCs decrease in the nearshore region, while increase in the offshore region. This is because stratification hindered the upward diffusion of bottom suspended sediment due to the lack of tidal mixing. As a result, most of the sediment can only be advected in the horizontal direction. The sediments in the surface layer transport upstream with fluxes of 0.05 ~ 0.1 kg/s and downstream with fluxes lower than 0.05 kg/s from the Yellow River mouth. The surface sediment fluxes in the south of Bohai Bay are westward with fluxes of 0 ~ 0.05 kg/s. In the bottom layer, the sediments transport onshore in the north side of the Yellow River mouth, downstream in the northwest of Laizhou Bay, and westward in the south of Bohai Bay. More sediments transport upstream without tidal forcing than with tidal forcing.

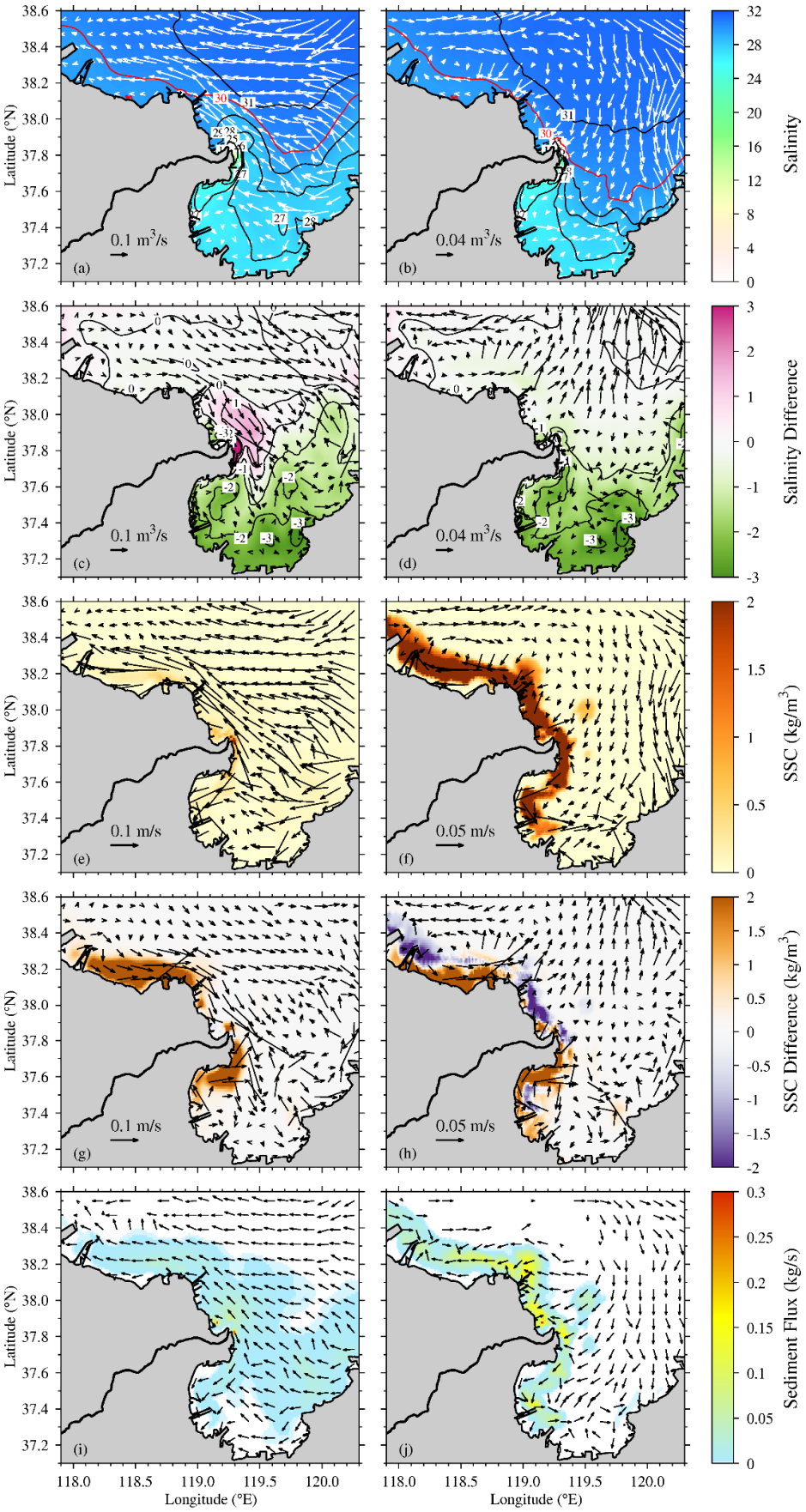
Latitude (°N)
Longitude (°E)
Salinity
Salinity Difference
SSC (kg/m3)
SSC Difference (kg/m3)
Sediment Flux (kg/s)
0.1 m3/s
0.04 m3/s
0.1 m/s
0.05 m/s
(a)
(b)
(c)
(d)
(e)
(f)
(g)
(h)
(i)
(j)

Figure 12. Distributions of residual unit width water flux and salinity (a, b), residual water velocity and SSC (e, f), residual unit width sediment flux (i, j) in Exp 1, and differences of residual unit width water flux and salinity (c, d), residual water velocity and SSC (g, h) of Exp 0 (control run) – Exp 1 (without tide) at surface layer (left panel) and bottom layer (right panel) during spring tide in December 2012 (arrows only signify direction, color signify the value of residual sediment flux in i and j).

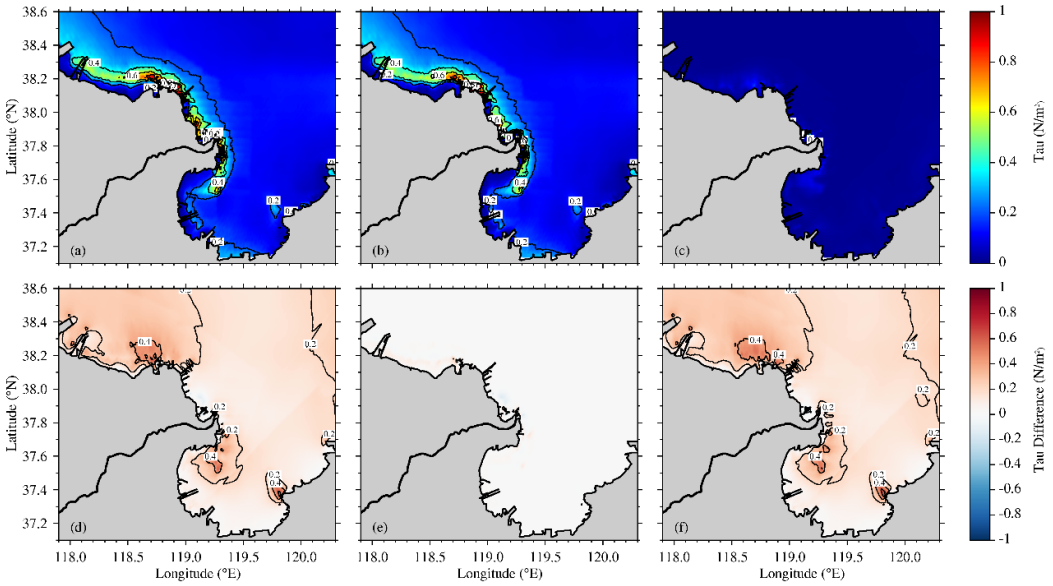

Figure 13. Distributions of total bottom shear stress (a), bottom shear stress induced by wave (b), bottom shear stress induced by tide (c) in Exp 1, and differences of total bottom shear stress (d), bottom shear stress induced by wave (e) and bottom shear stress induced by tide (f) of Exp 0 (control run) – Exp 1 (without tide) during spring tide in December 2012.

The residual water from the Yellow River mouth flows downstream across Sec 1 in the upper layer within 7 km away from the coast with velocities of about 0 ~ 8 m/s (Figure 14a). Out of 7 km, the residual water transports upstream in the upper layer and downstream in the lower layer. The surface along-section currents are shoreward with velocities of 5 ~ 8 m/s driven by the northwestward Ekman transport induced by

536 the northeasterly wind. The bottom currents flow onshore along Sec 1 driven by the
537 baroclinic gradient force. The low-salinity water transports downstream to Sec 1,
538 forming a salinity variance of 17 ~ 31. The water column is well-mixed in the surface
539 layer due to the wave mixing and stratified in the middle and bottom layer due to the
540 lack of tidal mixing. The difference between Exp 0 and Exp 1 indicates the effect of
541 tide. Tidal forcing induces more residual water transports downstream across Sec 1
542 within 28 km away from the coast. As a result, the salinity of Exp 0 in most areas
543 along Sec 1 especially in the bottom layer is lower than Exp 1. However, in the upper
544 layer, the salinity of Exp 0 with tidal forcing is higher than Exp 1 without tidal forcing.
545 This is caused by the mixing of bottom saline water with surface fresh water induced
546 by the tidal mixing. The salinity differences of Exp 0 and Exp 1 are about 0 ~ 4 in the
547 upper layer within 26 km and -2 ~ 0 in the bottom layer along Sec 1.

548 The SSCs along Sec 1 are about 0 ~ 3 kg/m^3 within 10 km away from the coast
549 with higher values in the bottom and declining upward. Due to the decrease of bottom
550 shear stress induced by tide, the SSCs of Exp 1 are reduced for about 0 ~ 2.5 kg/m^3
551 compared with Exp 0. The reduction of SSC is highest in the middle layer at about 3
552 km away from the coast as a result of the lack of tidal mixing and tide-induced
553 sediment resuspension.

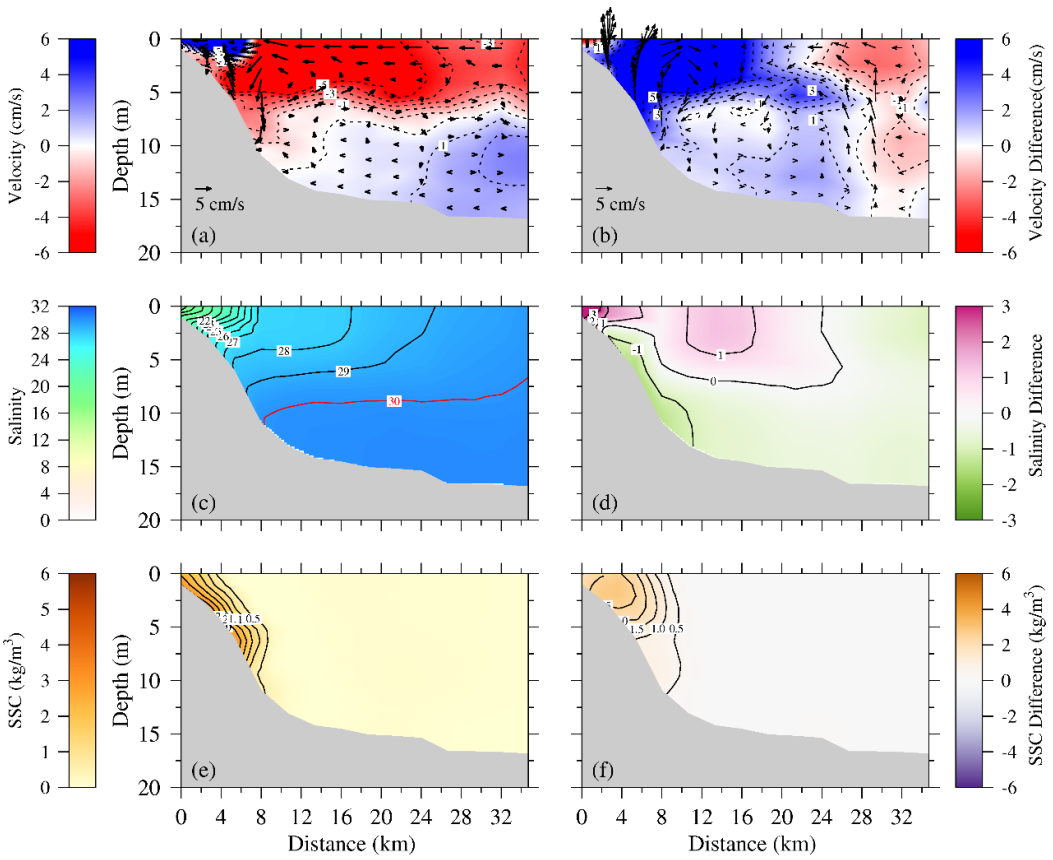

Figure 14. Vertical profile distributions of residual velocity (a), salinity (c) and SSC (e) in Exp 1, and differences of residual velocity (b), salinity (d) and SSC (f) of Exp 0 (control run) – Exp 1 (without tide) along Sec 1 during spring tide in December 2012 (arrows in (a, b) signify current vectors along section, and the contours signify current velocities perpendicular to the section (positive values indicate downstream current)).

4.2 The effect of wave on the transport of water and sediments

Exp 2 considered the effect of tide and excluded the wave forcing. The residual water velocities and fluxes are similar to Exp 0. Except for the central area of Bohai Sea, where wave induces northwestward transport in the surface layer, carrying more low-salinity water from the coast to the sea. As a result, the salinity of Exp 0 is about

565 0 ~ 1 lower than Exp 2. The salinity differences between Exp 0 and Exp 2 are higher
566 than 3 near the Yellow River mouth in the whole water column due to the mixing of
567 surface fresh water with bottom saline water induced by wave. As a result, more fresh
568 water extends upstream and downstream, resulting in the lower salinity in the
569 northwest side of the Yellow River mouth and in the center and on the northeast of
570 Laizhou Bay (Figure 15c, d).

571 Without wave forcing, the bottom shear stress induced by wave is zero (Figure
572 16b). The reduction of bottom shear stress is about 0 ~ 1 N/m^2 along the Yellow River
573 Delta. The maximum total bottom shear stress is about 0.2 N/m^2 near the Yellow
574 River mouth and on the downstream side, and about 0.4 N/m^2 in the south of Bohai
575 Bay. The bottom shear stress induced by tide also decreases for about 0 ~ 0.2 in the
576 south of Bohai Bay, from the Yellow River mouth downstream to the north of Laizhou
577 Bay, and in the east head of Laizhou Bay, as a result of the change of bottom water
578 current. The weaker bottom shear stress resuspends less sediment above bed. The
579 bottom SSCs decrease more than 2 kg/m^3 along the Yellow River Delta and the
580 surface SSCs decrease about 2 kg/m^3 from the Yellow River mouth downstream to the
581 north of Laizhou Bay and in the south of Bohai Bay (Figure 15g, h). As a result, the
582 suspended sediments are mostly in the south of Bohai Bay and from the Yellow River
583 mouth downstream to the north of Laizhou Bay with values of 0 ~ 1.5 kg/m^3. The
584 surface SSC is slightly lower than bottom SSC because tidal mixing enhances the
585 upward diffusion of bottom suspended sediments.

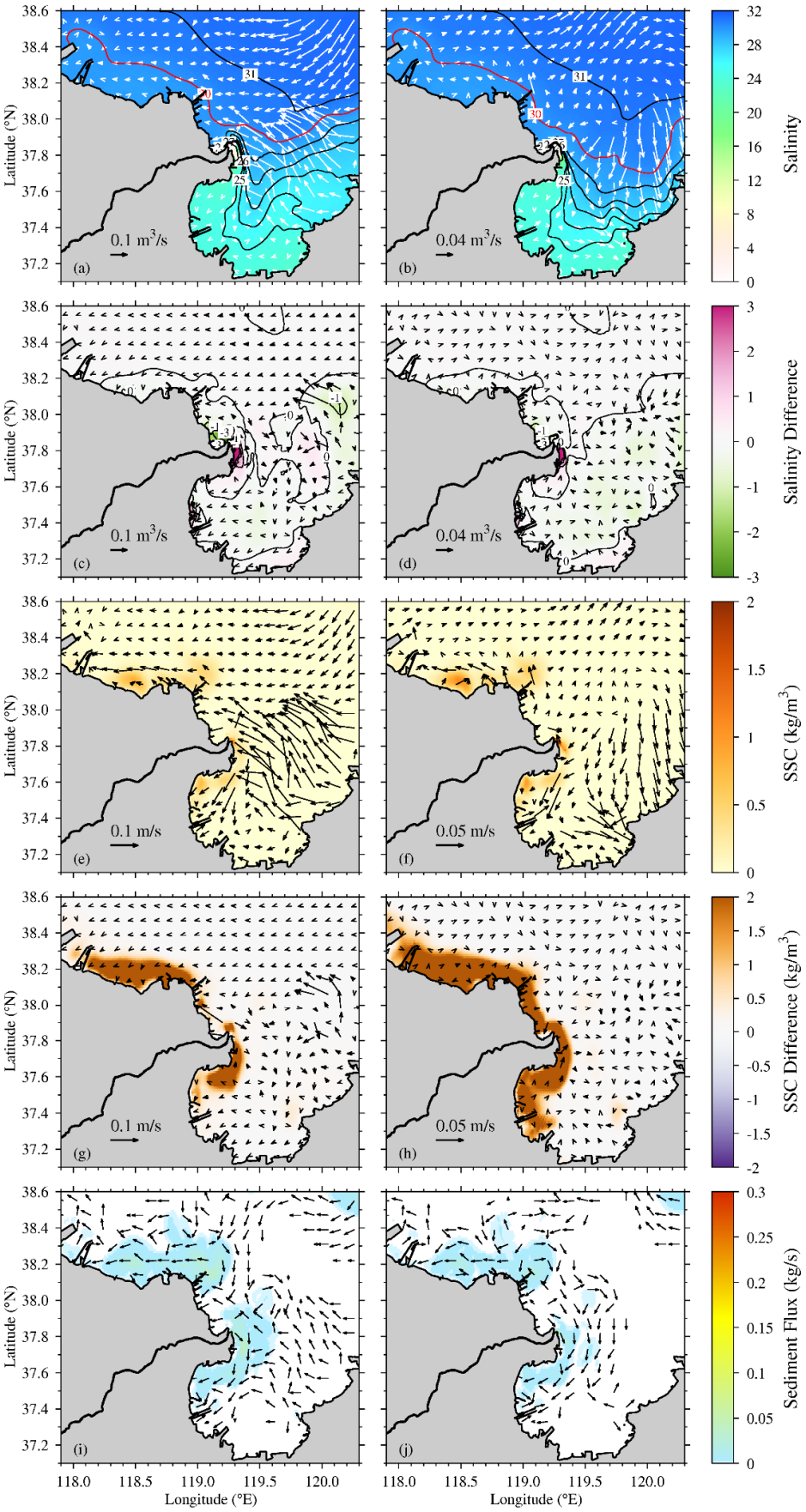
Latitude (°N)
Longitude (°E)
0.1 m³/s
0.04 m³/s
0.1 m/s
0.05 m/s
(a)
(b)
(c)
(d)
(e)
(f)
(g)
(h)
(i)
(j)
Salinity
Salinity Difference
SSC (kg/m³)
SSC Difference (kg/m³)
Sediment Flux (kg/s)

Figure 15. Distributions of residual unit width water flux and salinity (a, b), residual water velocity and SSC (e, f), residual unit width sediment flux (i, j) in Exp 2, and differences of residual unit width water flux and salinity (c, d), residual water velocity and SSC (g, h) of Exp 0 (control run) – Exp 2 (without wave) at surface layer (left panel) and bottom layer (right panel) during spring tide in December 2012 (arrows only signify direction, color signify the value of residual sediment flux in i and j).

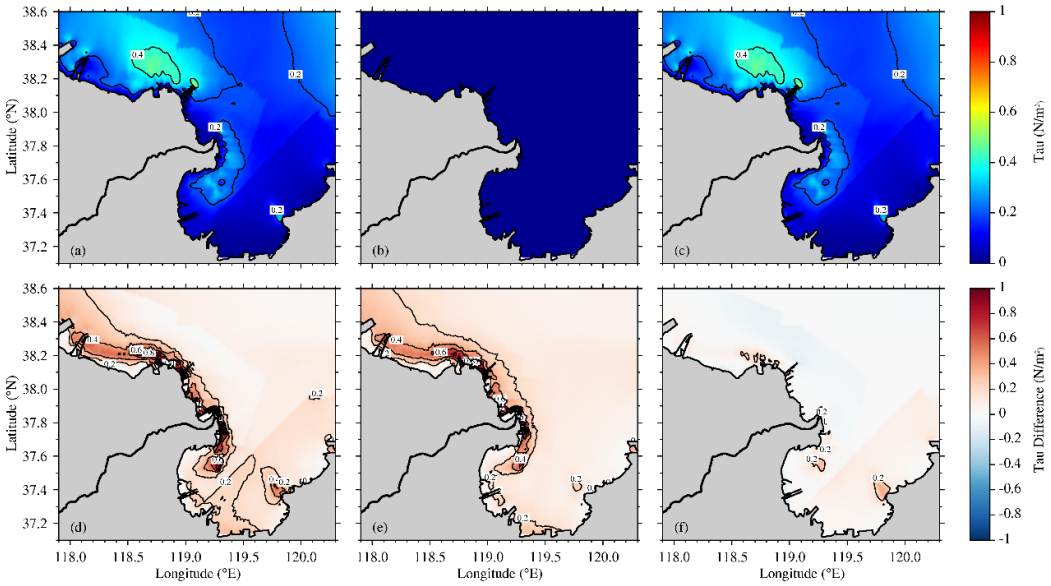

Figure 16. Distributions of total bottom shear stress (a), bottom shear stress induced by wave (b), bottom shear stress induced by tide (c) in Exp 2, and differences of total bottom shear stress (d), bottom shear stress induced by wave (e) and bottom shear stress induced by tide (f) of Exp 0 (control run) – Exp 2 (without wave) during spring tide in December 2012.

The SSCs are low, resulting in the weak sediment transport along the Yellow River Delta. The sediments from the Yellow River mouth transport downstream into Laizhou Bay with largest fluxes of 0.05 kg/s in the surface layer and 0.02 kg/s in the bottom layer. In the south of Bohai Bay, the sediment fluxes are westward with largest values of 0.06 kg/s in the surface layer and 0.03 kg/s in the bottom layer. Unlike Exp

603 1, the sediment fluxes in the surface layer are larger than in the bottom layer. Because
604 the surface SSCs are similar to the bottom SSCs and the surface water transport is
605 stronger than the bottom layer.

606 Without tidal forcing, the sediment transport of Exp 1 is weaker than Exp 0 with
607 tidal forcing. The sediment transport converges in the Yellow River mouth due to the
608 river sediment deposition. A part of river sediment transports downstream and settles
609 in the north of Laizhou Bay, forming a divergence area in the south side of river
610 mouth and a convergence area in Laizhou Bay (Figure 17a). The downstream
611 sediment transport weakened and the upstream sediment transport strengthened
612 without tidal forcing compared with Exp 0. Therefore, the sediment converges in the
613 north side of the river mouth with fluxes of 0.1 $g/m^2/s$. In the south of Bohai Bay, the
614 coastal sediments transport seaward and the marine sediments transport landward. As
615 a result, the sediment transport shows a divergence-convergence-divergence pattern
616 with fluxes of 0 ~ 0.05 $g/m^2/s$ from the coast to the sea. When the tidal forcing is
617 considered and wave forcing is excluded, the bottom shear stress decreases a lot and
618 less sediment suspends. As a result, the sediment transport weakens, except for the
619 river sediment deposition in the Yellow River mouth (Figure 17b). In other areas
620 along the Yellow River Delta, the sediment fluxes are lower than 0.06 $g/m^2/s$.

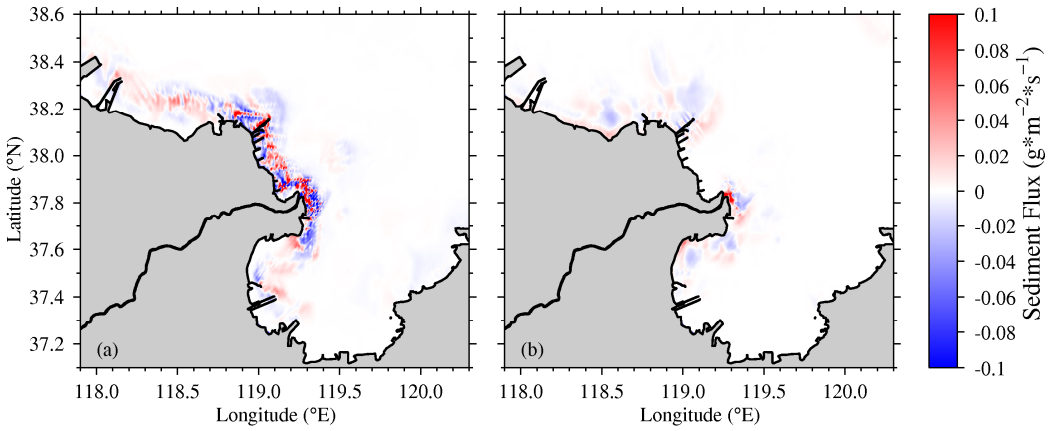

621

622 **Figure 17.** Distributions of sediment convergence and divergence during spring tide in December
623 2012 in Exp 1 (a) and Exp 2 (b) (positive value and red color indicate convergence, negative value
624 and blue color indicate divergence).

625 The wave induces a downstream transport of surface water within 5 km away
626 from the coast and an upstream transport between 5 ~ 10 km across Sec 1 (Figure
627 18b). Without wave forcing, the water column is well-mixed in the near-shore region
628 and stratified in the offshore area. The salinity within 8 km away from the coast is
629 lower than Exp 0 with wave forcing, meaning that the surface fresh water is mixed
630 with the bottom saline water due to the wave mixing. The water column of Sec 1 in
631 Exp 2 is vertically more mixed than Exp 1, indicating that tidal mixing is stronger
632 than wave mixing (Figure 18c). Due to the weak bottom shear stress in the absence of
633 wave forcing, the SSCs in Sec 1 decrease about 5 kg/m^3 in the nearshore bottom. The
634 maximum residual SSC in Sec 1 is higher than 0.5 kg/m^3 lower than 1 kg/m^3 between
635 2 ~ 7 km away from the coast in the bottom layer (Figure 18e).

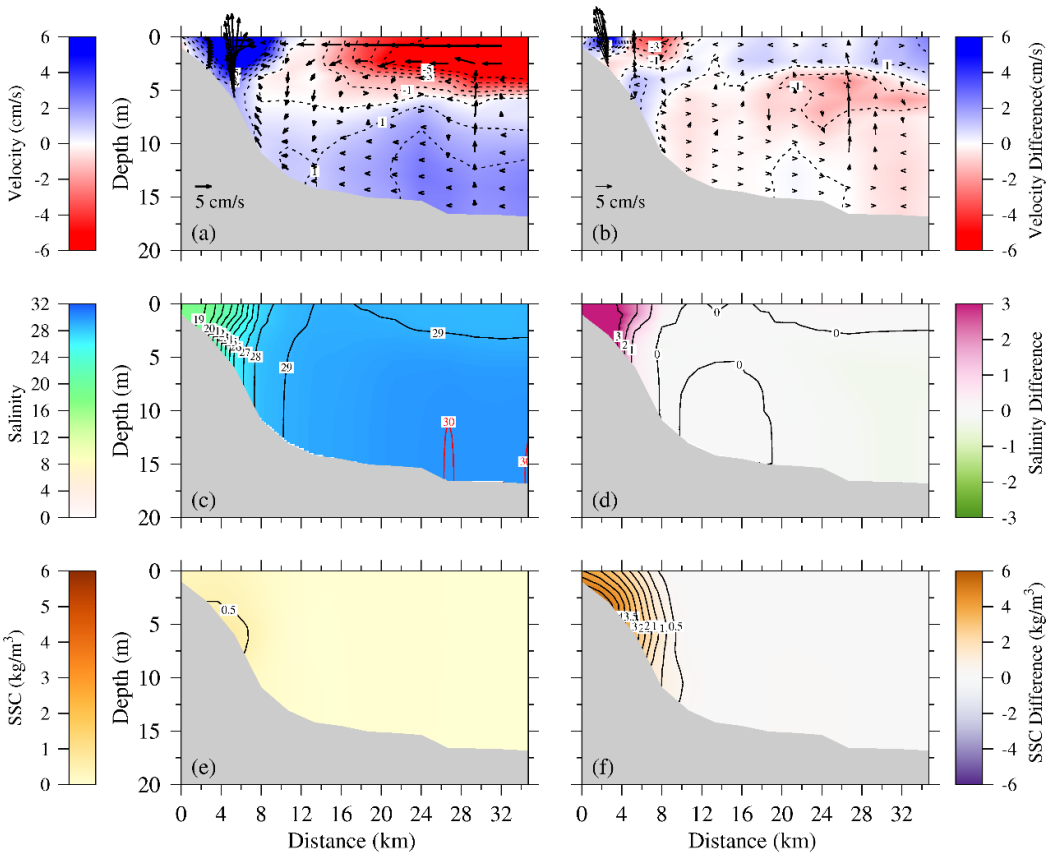

Figure 18. Vertical profile distributions of residual velocity (a), salinity (c) and SSC (e) in Exp 2, and differences of residual velocity (b), salinity (d) and SSC (f) of Exp 0 (control run) – Exp 2 (without wave) along Sec 1 during spring tide in December 2012 (arrows in (a, b) signify current vectors along section, and the contours signify current velocities perpendicular to the section (positive values indicate downstream current)).

The water, salt and sediment fluxes across Sec 1 in Exp 0, Exp 1 and Exp 2 are mainly in the downstream direction, especially in the beginning and ending of December 2012 (Figure 19). The water and salt transports of with and without wave are similar. However, the tidal forcing plays an important role in changing the water and salt fluxes. In Exp 1, the water and salt fluxes across Sec 1 enlarge due to the stratification in the water column without tidal mixing. During spring tide, the net

water fluxes in the upstream direction increase from 1.3×10^{8} m^3 to 1.9×10^{9} m^3, while the net salt fluxes increase from 5.0×10^{6} kg to 5.4×10^{7} kg, both rise one order of magnitude when removing tidal forcing from the experiment (Table 3). On the other hand, the wave forcing strengthens the net upstream transport of water and salt during spring tide. Without tidal forcing, the decreased bottom shear stress resuspends less sediment, resulting in weaker sediment transport across Sec 1. The net sediment flux across Sec 1 in Exp 0 during spring tide is 1.3×10^{9} kg in the downstream direction. Without tidal forcing, the sediment flux decreases to 1.9×10^{8} kg and turns to upstream direction. Without wave forcing, the sediment transport is weaker than without tidal forcing due to the lower bottom shear stress. Compared with Exp 0, the net sediment flux across Sec 1 in Exp 2 is in the same downstream direction and reduces to 3.7×10^{8} kg during spring tide .

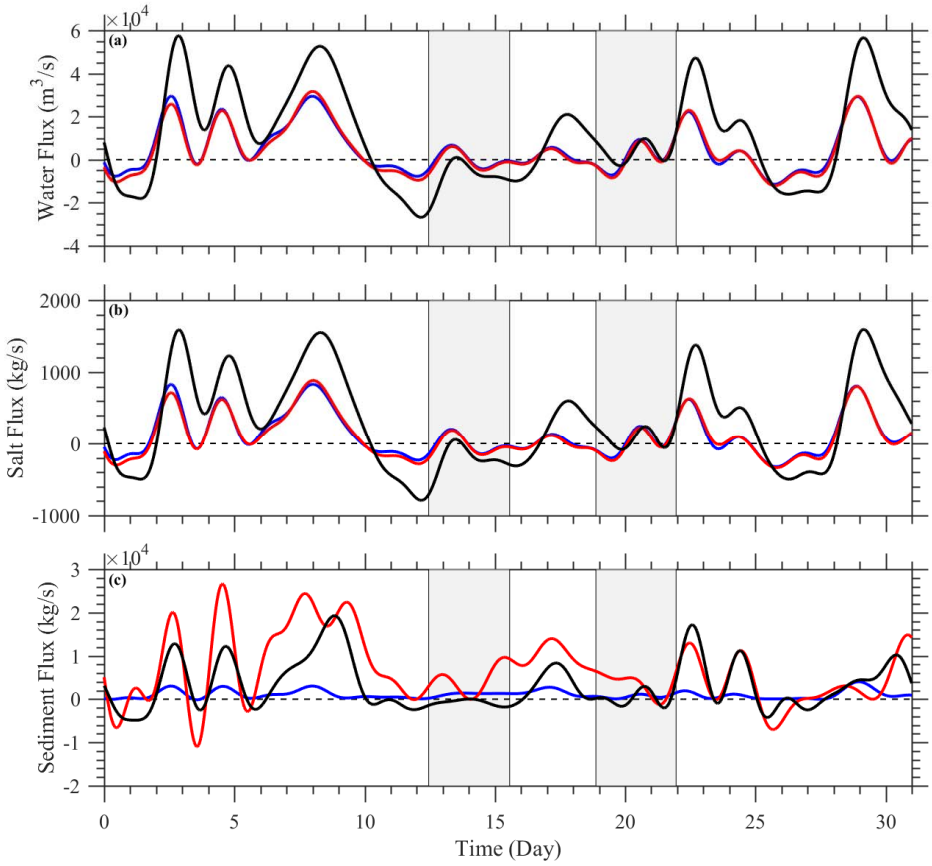

660

661 **Figure 19.** Temporal variations in water flux (a), salt flux (b) and sediment flux (c) across Sec 1 in

662 December 2012 in Exp 0 (red line), Exp 1 (black line) and Exp 2 (blue line); (positive values

663 indicate downstream transport; the left shadow indicates duration of spring tide, and the right

664 shadow indicates duration of neap tide).

665

666 **Table 3.** The net water flux (m^3), net salt flux (kg) and net sediment flux (kg) across Sec 1 during

667 spring tide in December 2012 in experiments (positive values indicate downstream transport)

	Exp 0	Exp 1	Exp 2
Net water flux (m^3)	-1.3×10^8	-1.9×10^9	7.2×10^7
Net salt flux (kg)	-5.0×10^6	-5.4×10^7	-4.8×10^5
Net sediment flux (kg)	1.3×10^9	-1.9×10^8	3.7×10^8

5. Conclusions

In this paper, the water and sediment transports from the Yellow River mouth are studied and the effects of tide and wave are discussed using a 3-D numerical model coupled with hydrodynamic and sediment module. The critical shear stress for erosion is calculated by the equation of Dou and later calibrated using measured and remote sensing retrieval SSC data. The model is validated with current, salinity, measured and remote sensing retrieval SSC data. The wave parameters simulated by SWAN model are validated with measured significant wave height and period data.

The water and sediment transports under the northeasterly prevailing wind in the Bohai Sea during spring tide in December 2012 are simulated. The fresh water off the Yellow River flows downstream, carrying the river sediment and suspended sediment into the Laizhou Bay. The bottom shear stress induced by wave is higher in the shallow water along the coast of Yellow River Delta. The bottom shear stress induced by tide is higher in the north of Laizhou Bay and south of Bohai Bay due to the larger water velocities.

Tidal forcing induces more fresh water transport downstream along the coast of Yellow River Delta. Without tidal forcing, the bottom shear stress is weak, resulting in less sediment resuspension in the bottom. The stratification in the water column hinders the upward diffusion of bottom suspended sediment due to the lack of tidal mixing. The wave forcing has little impact on the water transport. However, without wave forcing, the bottom shear stress decreases a lot, causing less suspended sediment along the Yellow River Delta, which also weakens the sediment transport. The wave

mixing is weaker than tidal mixing in the vertical direction. This paper explains the effects of tide and wave on the transport of water and sediments off the Yellow River mouth in winter.

Declaration of competing interest

The authors declare no competing interests.

Acknowledgments

This study was supported by the National Key Research and Development Program of China (No. 2017YFC0405503), and the National Natural Science Foundation of China (NSFC) (No. U1706214). We also acknowledge the anonymous reviewers for their valuable comments and suggestions. The sea surface wind data obtained from ECMWF are available at http://apps.ecmwf.int/datasets/. Open ocean boundary water flux, salinity data are provided by SODA at http://iridl.ldeo.columbia.edu/SOURCES/.CARTON-GIESE/.SODA/.v2p0p2-4/. Tidal constituents are obtained from the NaoTide data set (http://www.miz.nao.ac.jp/). The topographic data of the Bohai Sea are observational data from the Yellow River Water Commission. The remote sensing images of Landsat 8 OLI are downloaded from USGS (http://glovis.usgs.gov/).

References

Arakawa, A., and V. R. Lamb (1977), Computational design of the basic dynamical processes of the UCLA general circulation model, *General Circulation Models of the Atmosphere*, *17*, 173-265.

Bian, C., W. Jiang, and R. J. Greatbatch (2013), An exploratory model study of sediment transport sources and deposits in the Bohai Sea, Yellow Sea, and East China Sea, *Journal of Geophysical Research: Oceans*, *118*, 5908–5923.

Blumberg, A. F. (1994), A primer for ECOM-si, *Technical Report of HydroQual*, *Mahwah, New Jersey*, 66.

Blumberg, A. F., and G. L. Mellor (1987), A description of a threedimensional coastal ocean circulation model, *In: Heaps, N.S. (ed.), Coastal and Estuarine Science, Volume 4, Three-Dimensional Coastal Ocean Models. Washington, DC: American Geophysical Union*, 1-16.

Brand, A., J. R. Lacy, K. Hsu, D. Hoover, S. Gladding, and M. T. Stacey (2010), Wind-enhanced resuspension in the shallow waters of South San Francisco Bay: Mechanisms and potential implications for cohesive sediment transport, *Journal of Geophysical Research*, *115*, C11024.

Cao, Z., and Y. Wang (1994), *Hydrodynamic and sediment transport numerical simulation (in Chinese)*, Tianjin University Press, Tianjin, China.

Chapman, D. C., and S. J. Lentz (1994), Trapping of a coastal density front by the bottom boundary layer, *Journal of Physical Oceanography*, *24*(7), 1464-1479.

Chen, C., J. Zhu, L. Zheng, E. Ralph, and J. W. Budd (2004), A Non-orthogonal

732 Primitive Equation Coastal Ocean Circulation Model: Application to Lake
733 Superior, *Journal of Great Lakes Research*, *30*(supp-S1), 41-54.
734 Chen, S. (2001), Seasonal, neap-spring variation of sediment concentration in the
735 joint area between Yangtze Estuary and Hangzhou Bay, *Science in China Series*
736 *B: Chemistry*, *44*, 57-62.
737 Cheng, X., J. Zhu, and S. Chen (2021a), Dynamics of the extension of the Yellow
738 River plume in the Bohai Sea, *Continental Shelf Research*, *222*(9), 104438.
739 Cheng, X., J. Zhu, and S. Chen (2021b), Extensions of the river plume under various
740 Yellow River courses into the Bohai Sea at different times, *Estuarine, Coastal*
741 *and Shelf Science*, *249*(107092).
742 Cui, B. L., and X.-Y. Li (2011), Coastline change of the Yellow River estuary and its
743 response to the sediment and runoff (1976–2005), *127*(1-2), 0-40.
744 Dou, G. (1999), Incipient Motion of Coarse and Fine Sediment (in Chinese), *Journal*
745 *of Sediment Research*, *6*, 1-9.
746 Doxaran, D., J. M. Froidefond, and P. Castaing (2002), A reflectance band ratio used
747 to estimate suspended matter concentrations in sediment-dominated coastal
748 waters, *International Journal of Remote Sensing*, *23*(23), 5079–5085.
749 Fan, H., and H. Huang (2005), Changes in Huanghe (Yellow) River estuary since
750 artificial re-routing in 1996, *Chinese Journal of Oceanology and Limnology*,
751 *23*(3), 299-305.
752 Fan, H., H. Huang, T. Q. Zeng, and K. Wang (2006), River mouth bar formation,
753 riverbed aggradation and channel migration in the modern Huanghe (Yellow)

754 River delta, China, *Geomorphology*, *74*, 124– 136.
755 Fettweis, M., M. Sas, and J. Monbaliu (1998), Seasonal, Neap-spring and Tidal
756 Variation of Cohesive Sediment Concentration in the Scheldt Estuary, Belgium,
757 *Estuarine, Coastal and Shelf Science*, *47*, 21-36.
758 Geyer, W. R. (1993), The importance of suppression of turbulence by stra tification on
759 the estuarine turbidity maximum, *Estuaries*, *16*, 113 – 125.
760 Han, Q. (1997), The distribution and application of sediment dry density (in Chinese),
761 *Journal of Sediment Research*, *2*, 10-16.
762 Huang, S., N. Han, and X. Zhong (1980), Analysis of siltation at mouth bar of the
763 Yangtze River estuary, *Proceedings of the International Symposium on River*
764 *Sedimentation, Paper C6, Chinese Society of Hydraulic Engineering, Beijing,*
765 *China*.
766 Kong, D., C. Miao, A. G. L. Borthwick, Q. Duan, H. Liu, Q. Sun, A. Ye, Z. Di, and W.
767 Gong (2015), Evolution of the Yellow River Delta and its relationship with
768 runoff and sediment load from 1983 to 2011, *Journal of Hydrology*, *520*,
769 157-167.
770 Li, G., Z. Tang, S. Yue, K. Zhuang, and H. Wei (2001), Sedimentation in the shear
771 front off the Yellow River mouth, *Continental Shelf Research*, *21*, 607-625.
772 Li, G., H. Wei, Y. Han, and Y. Chen (1998a), Sedimentation in the Yellow River delta,
773 part I: flow and suspended sediment structure in the upper distributary and the
774 estuary, *Marine Geology*, *149*, 93-111.
775 Li, G., H. Wei, S. Yue, Y. Cheng, and Y. Han (1998b), Sedimentation in the Yellow

River delta, part II: suspended sediment dispersal and deposition on the subaqueous delta, *Marine Geology*, *149*, 113-131.

Liang, B., H. Li, and D. Lee (2008), Bottom shear stress under wave-current interaction, *Journal of Hydrodynamics*, *20*(1), 88-95.

Lin, J., and A. Y. Kuo (2001), Secondary turbidity maximum in a partially mixed microtidal estuary, *Estuaries*, *24*, 707 – 720.

Liu, G., and S. Cai (2019), Modeling of suspended sediment by coupled wave-current model in the Zhujiang (Pearl) River Estuary, *Acta Oceanologica Sinica*, *38*(7), 22-35.

Liu, Y., P. Maccready, B. M. Hickey, E. P. Dever, and N. S. Banas (2009), Evaluation of a coastal ocean circulation model for the Columbia River plume in summer 2004, *Journal of Geophysical Research Oceans*.

Long, C. M., and T. M. Pavelsky (2013), Remote sensing of suspended sediment concentration and hydrologic connectivity in a complex wetland environment, *Remote Sensing of Environment*, *129*, 197–209.

Luettich, R. A. J., D. R. F. Harleman, and L. Somlyódy (1990), Dynamic behavior of suspended sediment concentrations in a shallow lake perturbed by episodic wind events, *Limnology and Oceanography*, *35*(5), 1050-1067.

Lv, X., D. Yuan, X. Ma, and J. Tao (2014), Wave characteristics analysis in Bohai Sea based on ECMWF wind field, *Ocean Engineering*, *91*, 159-171.

Maréchal, D. (2004), A soil-based approach to rainfall-runoff modeling in ungauged catchments for England and Wales (PhD thesis), *Cranfield, UK: Cranfield*

798 *University*.
799 Martin, J. M., J. Zhang, M. C. Shi, and Q. Zhou (1993), Actual flux of the Huanghe
800 (Yellow River) sediment to the western Pacific Ocean, *Journal of Sea Research*,
801 *31*(93), 243-254.
802 Mehta, A. J., and W. H. McAnally (2008), Fine grained sediment transport,
803 *Sedimentation Engineering: Processes, Management, Modeling, and Practice*,
804 253-307.
805 Mellor, G. L., and T. Yamada (1974), A Hierarchy of Turbulence Closure Models for
806 Planetary Boundary Layers, *Journal of the Atmospheric Sciences*, *31*(7),
807 1791-1806.
808 Mellor, G. L., and T. Yamada (1982), Development of a turbulence closure model for
809 geophysical fluid problems, *Reviews of Geophysics and Space Physics*, *20*(4),
810 851-875.
811 Murphy, A. H. (1988), Skill Scores Based on the Mean Square Error and Their
812 Relationships to the Correlation Coefficient, *116*(12), 990-991.
813 Pang, J. Z., and S. H. Si (1979), Evolution of the Yellow River mouth: I. Historical
814 shifts, *Oceanologia Et Limnologia Sinica*, *10*(2), 136–141.
815 Qin, Y. S., and F. Li (1983), Study of influence of sediment loads discharged from
816 Huanghe River on sedimentation in Bohai Sea and Huanghai Sea., paper
817 presented at International Symposium on Sedimentation on the Continental Shelf,
818 with Special Reference to East China Sea, Hangzhou, China.
819 Ralston, D. K., W. R. Geyer, and J. A. Lerczak (2010), Structure, variability, and salt

820 flux in a strongly forced salt wedge estuary, *Journal of Geophysical Research*
821 *Atmospheres*, *115*(C6).
822 Sanford, L. P. (1994), Wave-forced resuspension of upper Chesapeake Bay muds,
823 *Estuaries Coasts*, *17*(1), 148-165.
824 Scully, M. E., and C. T. Friedrichs (2003), The influence of asymmetries in overlying
825 stratification on near-bed turbulence and sediment suspension in a
826 partially-mixed estuary, *Ocean Dynamics*, *53*, 208 – 218.
827 Scully, M. E., and C. T. Friedrichs (2007), Sediment pumping by tidal asymmetry in a
828 partially mixed estuary, *Journal of Geophysical Research*, *112*, C07028.
829 Signell, R. P., R. C. Beardsley, H. C. Graber, and A. Capotondi (1990), Effect of
830 wave-current interaction on wind-driven circulation in narrow, shallow
831 embayments, *Journal of Geophysical Research*, *95*, 9671-9678.
832 Simpson, J. H., J. Brown, J. Matthews, and G. Allen (1990), Tidal straining, density
833 currents, and stirring in the control of estuarine stratification, *Estuaries*, *13*,
834 125-132.
835 Smagorinsky, J. (1963), General circulation experiments with the primitive equations:
836 I. The basic experiment, *Monthly Weather Review*, *91*(3), 99-164.
837 Sun, X. (2013), The impact of wave on the sediment erosion and deposition near the
838 Yellow River mouth, Ocean University of China, Qingdao.
839 Traykovski, P., W. R. Geyer, and C. Sommerfield (2004), Rapid sediment deposition
840 and fine-scale strata formation in the Hudson estuary, *Journal of Geophysical*
841 *Research*, *109*, F02004.

van Leussen, W. (1988), Aggregation of particles, settling velocity of mud flocs: A review, *Physical Processes in Estuaries*, *edited by J. Dronkers and W. van Leussen*, 347 – 403.

Wang, H., Z. Yang, Y. Li, Z. Guo, X. Sun, and Y. Wang (2007), Dispersal pattern of suspended sediment in the shear frontal zone off the Huanghe (Yellow River) mouth, *Continental shelf research*, *27*, 854-871.

Wang, N. (2014), Sedimentary dynamics process and topographic evolution in the modern Yellow River Mouth, Ocean University of China, Shandong.

Wolanski, E., B. A. King, and D. Galloway (1995), Dynamics of the turbidity maximum in the Fly River estuary, Papua New Guinea, *Estuarine, Coastal and Shelf Science*, *40*(3), 321-337.

Wu, H., and J. Zhu (2010), Advection scheme with 3rd high-order spatial interpolation at the middle temporal level and its application to saltwater intrusion in the Changjiang Estuary, *Ocean Modelling*, *33*(1-2), 33-51.

Wu, T., and H. Wu (2018), Tidal Mixing Sustains a Bottom-Trapped River Plume and Buoyant Coastal Current on an Energetic Continental Shelf, *Journal of Geophysical Research: Oceans*, *123*(11), 8026-8051.

Yu, Y., H. Wang, X. Shi, X. Ran, T. Cui, S. Qiao, and Y. Liu (2013), New discharge regime of the Huanghe (Yellow River): Causes and implications, *Continental Shelf Research*, *69*, 62-72.

Zhan, C., J. Yu, Q. Wang, Y. Li, D. Zhou, Q. Xing, and X. Chu (2017), Remote Sensing Retrieval of Surface Suspended Sediment Concentration in the Yellow

River Estuary, *Chinese Geographical Science*, *27*(6), 934-947.

Zhu, J. (2003), Ocean numerical calculation method and numerical model, *China Ocean Press, Beijing*, (in Chinese with English Abstract).